A STUDY OF EFFECT OF BOND LENGTH ON BOND STRENGTH OF FUSED DEPOSITION MODELING PARTS USING TRANSIENT HEAT TRANSFER ANALYSIS

by

JUNAID BAIG

Presented to the Faculty of the Graduate School of

The University of Texas at Arlington in Partial Fulfillment

of the Requirements

for the Degree of

MASTER OF SCIENCE IN MECHANICAL ENGINEERING

THE UNIVERSITY OF TEXAS AT ARLINGTON

AUGUST 2018

Acknowledgments:

I would like to thank Dr. Robert Taylor for his constant motivation and unconditional support by providing me with valuable feedback with his abundant knowledge and wisdom. I would like to acknowledge Dr. Endel Iarve for being on the committee and giving important insights about the model. I am deeply thankful to Dr. Ankur Jain and Mr. Darshan Ravoori for providing experimental data and valuable inputs during the course of my project. I would also extend my gratitude towards Dr. Hyejin Moon for providing access to COMSOL Multiphysics software through her lab. Ms. Munmun Nahar and Mr.Ritul Gandhi have helped me by giving their insights about the software and I am grateful to them for the same. I would also like to thank Mr. Vatsal Joshi for his help with MATLAB software. Finally, I would like to thank Dr. Adnan for giving me access to his lab for carrying out the tensile experiments and Mr. Rane for performing them. I am very grateful and thank each and every one of the above-mentioned professors and colleagues for helping me in the successful completion of my master's thesis.

Abstract

It is important to understand the mechanical properties of bonding between adjacent layers of 3D printed parts built by Fused Deposition Modeling process (FDM). The bonding process is highly non-linear and depends on various geometric and thermal process parameters. This work aims to quantify the degree of bonding by calculating the bond potential between the extruded layers using finite element (FE) heat transfer analysis. Successive transient analyses were carried out using this model by constantly updating the boundary conditions and geometric model during the deposition of the extruded bead. Temperatures at critical points were calculated over a period to calculate the bond potential and analyze the degree of bonding between layers printed in the z-axis. Furthermore, geometry and heat transfer coefficient were altered to investigate their influence on the bond potential. Finally, the experimental analysis was carried out by printing tensile specimens according to the FE model to investigate any relationship between the calculated bond potential and strength of the FDM parts.

List of Figures

List of Tables

Chapter 1 Introduction

Fused deposition modeling is one of the noteworthy processes known in the additive manufacturing spectrum. The minimalistic cost associated with polymer extrusion in fused deposition modeling (FDM) makes it accessible to the masses. However, certain limitations like the presence of voids and improper bonding of the polymer [2] makes one reluctant to use FDM for industrial applications, especially parts which have a larger build height. In order to tackle these problems, it becomes imperative to study the bonding between the layers which takes place during the extrusion process and the process parameters affecting the bonding.

This work aims to study this phenomenon by capturing the extrusion environment in FDM; the geometry, the working temperature and the changes that take place during the build. A numerical approach comprising of successive transient heat transfer analysis in finite element (FE) software was used to calculate the temperature history between the bonded layers after the extrusion takes place. This temperature history serves to be an important parameter to predict the degree of bonding by calculation of *bond potential*. The *bond potential* can be used to quantify the degree of bonding between layers and thereby, serve as a bridge between the structural and thermal aspects of the process and thus, we can understand the bonding in FDM parts. The study comprises of two models of varying lengths and the effect of bond potential on different length. Furthermore, the investigation of bond potential with varying heat transfer coefficient was also studied. Thus, a parametric study in the form of the geometry and the heat transfer coefficient as process parameters to understand better the degree of bonding between two successive layers was performed.

Chapter 2 Background

2.1 Additive manufacturing

Additive manufacturing (AM) technology or 3D printing has shown enormous potential as a post-modern manufacturing process. AM may be defined as "—A process of joining materials to make objects from 3D model data, usually layer upon layer, as opposed to subtractive manufacturing methodologies" [1]. Initially, AM was known as rapid prototyping (RP), since its main objective was to rapidly create a system or a part before launching the product commercially [2]. Over the period of time, this notion has changed. Today these technologies are not just limited to prototyping but are used to generate the final product itself. AM technologies are known for their ability to produce complex shapes and contours, which would be difficult to reproduce using a conventional manufacturing process. The manufacturing takes less overall time than conventional manufacturing processes and is devoid of human labor whilst the part is being manufactured leading to increased accuracy and tighter tolerances.

The AM processes may be classified into seven different categories. This data has been listed in detail by the ASTM F42 committee [3]. Each process differs from the other process on the basis of the deposition of the layers and the also the process by which the successive layers bond with each other. They also differ on the basis of build materials and their state (Liquid, filaments, powdered state or solid sheet) before they undergo manufacturing. All these details have been listed in Table1.

Table 1: Types of the additive manufacturing process [10]

Sr no	Process category	Process technology	Material	Manufacturer
1	Vat photo polymerization	SLA	UV curable resins Waxes Ceramics	Asiga 3D Systems EnvisionTEC Rapid shape DWS Lithoz
2	Material Jetting	Multi-jet modeling	Waxes UV curable resins	3D systems Stratasys Solidscape
3	Binder jetting	3DP	Composites Polymers Cermaics Metals	3D systems Voxeljet ExOne
4	Metal extrusion	FDM, FFF,MEM	Thermoplastics waxes	Stratasys MakerBot RepRap Bits from Bytes Fabbster Delta Micro Factory Corporation Beijing Tiertime Choc Edge Essential Dynamics Fab@Home
5	Powder bed fusion	1. SLS 2. SLM 3. EBM (electron beam melting)	1.Thermoplastics, Metals 2. Metals 3. Metals	1.EOS, Blueprinter,3D systems, 3Geometry, Matsuura, 3D Systems/Phoenix 2. EOS, SLM Solutions, Concept Laser, 3D Systems, Realizer, Renishaw 3. Arcam, Sciaky
6	Sheet lamination	LOM	Paper Metals Thermoplastics	Mcor Technologies FAbrisonic Solido
7	Direct energy deposition	1. LMD/LENS 2. EBAM (electron beam AM)	1. Metals 2. Metals	1. Optomec, DM3D, Irepa Laser. 2. Sciaky

2.1.1Fused deposition modeling:

The following thesis focuses on the process of the Fused deposition modeling. Fused deposition modeling (FDM) is also known as Fused filament fabrication (FFF), Filament deposition technique (FDT) or Melt extrusion manufacturing [4]. As the names suggest, it involves layer by layer deposition of a material in its molten form and is fused to its adjacent layers to create a solid structure. FDM was mainly known as rapid prototyping technology involving 3D rudimentary designs for visual aid or presentation [2]. Recently, they are also used as the final part, provided they are met with strict functional design requirement for mechanical properties and dimensional tolerances [2]. Some of the advantages of parts built by FDM are the robust mechanical properties and the range of materials that have been adopted as feedstock. Parts made using FDM are among the strongest for any polymer-based additive manufacturing process [2].

Ever since the FDM patent was awarded to Stratasys in 1992, the company has flourished to a point where FDM machines were sold more than any other AM machine type in the world. According to the Wohler's report of 2004 FDM machines alone sold as many machines as the whole AM machines combined [5]. In 2006 Stratasys sold 54.7 % (1723) machines compared to the rest of the AM machines. The industrial line of FDM system from Stratasys cost between $100,000-$500,000. Initial patent expiration from Stratasys in 2007 brought an impetus in the availability of machines, globally and we could observe an exponential rise. The E-Print and F-Print machines of a Chinese company Beijing Yinhua cost about $10,000-$72,000 and are currently available in the Asian Markets. FDM industry has also acquired small-scale 3D printers which are available as cheap as $1,500-$5,000 with limited materials [6]. According to Wohler's report of 2015, the sales of FDM machines under $5000 have risen from a mere 66 in 2007 to 139,584 in 2014 [7]

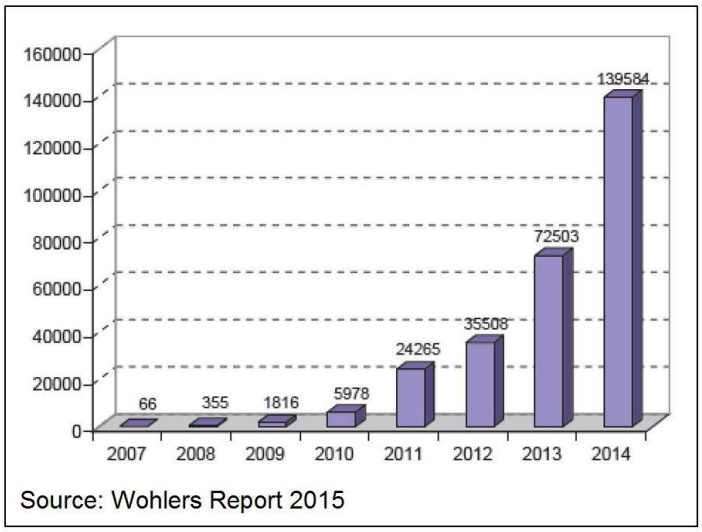

Figure 1 Rise in sales of FDM machines (under 5000$) from 2007 to 2014 [7]

.

2.1.2 Applications

Rapid Prototyping is the main application of FDM technology. The RP applications have influenced aerospace, automotive, dental, medical, and even consumer products. This impact will keep growing and benefit more industries over a period of time. However, with continuous improvements made in the technologies, industries are trying to leverage the advantages of FDM to acquire finished products thereby bypassing the conventional manufacturing processes. Some of the significant applications of FDM are:

1. Volvo has incorporated 3D printed jigs, tools and assembly aids for its engine using the Fortus machine which decreases the lead time by 94%. As plastics are the main materials used as a replacement for metal some parts cost €1 per cubic centimeter which is only 1% of the price as compared to being manufactured in metal [8]

Figure 2: Jigs and Fixtures additively manufactured by Volvo [8]

2. Genesis Systems Group is known for building robotic, waterjet cutting systems for trimming composite parts. They incorporated a design where, instead of using a robotic arm to move the waterjet cutter, the waterjet was kept fixed and the robot moved the part. However, this approach was difficult to implement because they had to use a custom gripper to hold and manipulate the parts. It took nearly $8,000 and 20 days to make those custom parts with CNC. On shifting to FDM they reduced the time and weight of the part considerably. It took them only 3 days to 3D print their ‘End of arm tools’ and reduced the weight from 35lbs to only 3lbs.[9]

Figure 3: A lightweight FDM end effector by Genesis Systems Group [9]

3. Melron Corporation, a manufacturer of window and door hardware shifted from traditional manufacturing of sand casting patterns to additively manufactured

patterns. Cost of manufacturing of the patterns reduced from 5000$ to 2000$ and the delivery time reduced from 3 weeks to 1.5 weeks. They also used the FDM printers to manufacture the gate and the runner system, thus, saving an additional 6 hours of manual work for each match plate[9]

Figure 4 Sand casting through additive manufacturing [9]

2.1.3 Need for research

From the above examples, it is evident that FDM is being widely acknowledged by different sectors. However, there are numerous challenges which need to be addressed in order to generate high fidelity parts. These challenges can be classified as follows: Fewer compliant materials, effects of residual stresses and stair stepping effect causing inconsistent parts and lack of qualification and certification methodologies for AM processes. [10].

In order to tackle the above issues, it is imperative to understand the processes intrinsically. There is a huge need of research in modeling, sensing, control and process innovation to understand the AM systems and thereby provide a novel and optimized solutions to improve quality, fidelity, and integrity of these parts. [10]

2.2 Operation:

Mechanism of an ideal FDM process involves a material feedstock in the form of a solid filament which is fed to the liquefier assembly. This liquefier assembly comprises of a tube secured at the inlet, the pinch rollers, the heater coils and an extruder tip secured at the outlet. The pinch rollers attached to motor revolve under constant torque and provide constant pressure at which the filament enters in the liquefier assembly [12]. The filament is melted in the heated liquefier with the help of heater coils wrapped around the chamber which provides constant temperature [12] and the polymer achieves a viscoelastic state. The extrusion takes place due to 3 major factors; The pressure drops, the nozzle geometry, and the material viscosity [4]. The materials used in FDM are primarily amorphous polymers [2]. Hence the viscosity increases with an increase in temperature [4]. The nozzle geometry determines the shape of the layer deposited and the pressure drop between the chamber and the surrounding atmosphere causes the flow of material from the extruder to a bed where it can solidify. The liquefier assembly moves in the horizontal x–y plane as the material is deposited on a build surface in form of a 2D sliced layer. Correspondingly it also moves in the z-direction after the deposition of each layer in x-y direction.

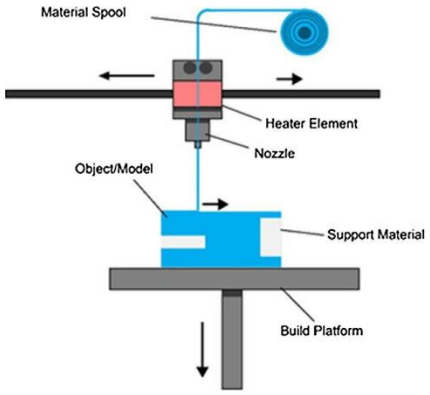

Figure 5: FDM schematic diagram[23]

2.3 Materials:

Amorphous polymers are mainly used in FDM. The primary reason for this is that the extrusion takes place in form of a viscous paste which would later solidify into the desired shape (extruder geometry). Amorphous polymers do not have a distinct melting point instead they have a characteristic glass transition temperature (T_g) [2]. Hence in the heating chamber, the polymer is heated above the glass transition temperature where the material increasingly softens, and viscosity lowers with an increase in temperature. Thus, a viscoelastic state is achieved by polymers after which they can be easily extruded and under a pressure high enough that their shape will be largely maintained after extrusion and enabling them to solidify spontaneously below glass transition temperature. It is also important for the material to bond with the adjacent road as a new layer or previously extruded material bonds with it.

The most common material used is ABS (Acrylonitrile butadiene styrene). However, there are various blends of ABS are commercially available depending upon the material properties, application, colors etc. An updated version of ABS is the ABSplus which works in all the platforms of Stratasys machines and is most widely used. Other blends of ABS include ABS-M30i [13] which is used for dental applications. ABSi is more frequently used for translucent parts and they provide similar strength as compared to ABS. ABSi has its application mainly in the RP and consumer products [14]. ABS-M30 is mostly used for RP however, it also has application as moderate requirement parts which include jigs, fixtures, manufacturing tools, prototyping, and production parts [15]. Table 2 enlists the list of material properties of ABS and its blends that are available [2].

Table 2: Material properties of ABS and its Blends [2]

Property	ABS	ABSi	ABSplus	ABS/PC
Tensile strength(MPa)	22	37	36	34.8
Tensile modulus(MPa)	1,627	1,915	2,265	1,827
Elongation (%)	6	3.1	4	4.3
Flexural strength(MPa)	41	61	52	50
Flexural modulus(MPa)	1,834	1,820	2,198	1,863
IZOD impact (J/m^2)	106.78	101.4	96	123
Heat deflection at 66 psi (^oC)	90	87	96	110
Heat deflection at 264 psi (^oC)	76	73	82	96
Thermal expansion (in./in./F)	5.60E-05	6.7E-6	4.90E-05	4.10E-5
Specific gravity	1.05	1.08	1.04	1.2

Other variants include PC based variants formulated by ISO 10993 and USP Class VI requirements. ULTEM 9085 is a sophisticated material variant used in FDM [11]. It has its main application in aerospace due to its favorable FST ratings. The Polyphenylsulfone has its application (low-volume injection molds, under-hood automotive scenarios, and heat, chemical, plasma, and radiation sterilization.) which require improved heat deflection(230^{o}C) [2]. PLA is another thermoplastic, similar to ABS which is widely used. It is eco-friendly, easy to print and readily available [16]

2.4 Bonding

Bonding basically signifies the adhesion between two extruded beads resulting in layer by layer construction of the actual 3D part. The bonding of the extruded bead is a significant phase as it will determine the fidelity of the part. Hence, it is important to understand the intricacies of bonding and cooling of the road in FDM. Effective bonding will lead to good quality parts with the least defects. Bonding takes place between: a) the extruded bead and the adjacent bead in the same layer (x-y axis), b) the extruded bead and an adjacent bead above previously extruded bead(z-axis). Bonding between two beads depends primarily on the material and its thermal factors. Heat transfer coefficient, thermal conductivity, and specific heat of the material play key factors in determining

optimal operating conditions. Furthermore, it also depends on the cooling of the roads, process parameters and the geometry of the road.

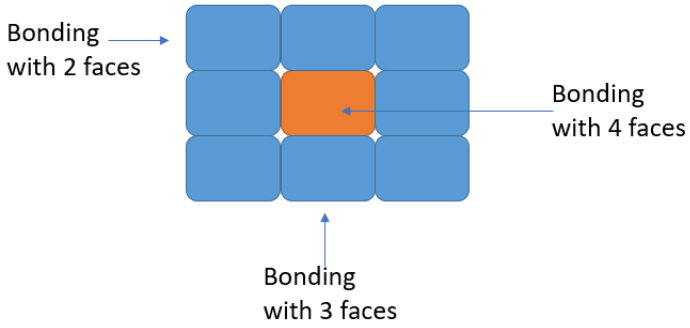

Figure 6: Oblong shaped extruded layers and types of bonding

Process parameters include the liquefier temperature, the environment temperature, speed of printing, infill, and the glass transition temperature (T_g). Road bonding takes place with the help of the sintering process which occurs through a viscous flow mechanism [17]. For sintering to take place, the temperature of the molten polymer should be above T_g. Hence the temperature is maintained well above T_g (230^{o}C-270^{o}C) as it extrudes. As discussed before the polymer solidifies below T_g (almost 105^{o}C for ABS) [18]. Thus, higher extrusion temperature enables bonding with the previously extruded bead. The process of sintering (bonding) involves energy supply to the bead by the extrusion head. Depending on the type of printer the ambient environment changes. It could be around 22^{o}C-25^{o}C if the machines are open (MakerBot and other small-scale printers) or it could be between 30^{o}C-50^{o}C if it is enclosed. Infill is a repetitive pattern or a structure that is print inside any part. There is a variety of patterns available along with the density of the infill. Infill significantly affects the weight and the performance of any part. The speed of printing is the speed at which the gantry moves across the bed as it extrudes the molten polymer.

The quality of bonding depends on this energy supplied by the extrusion head. There is always the danger of obtaining “spaghetti patterns” [19] from fused deposition if the bonding is inadequate. If the energy supplied is insufficient it would lead to a distinct boundary between the new and the previous bead. This could result in defects like voids, cracks which could lead to premature failures in parts. Too much energy, on the other hand, may cause the previous bead to flow, causing a poorly defined part [19]. Thus, there is a huge need to understand the physics and dynamics of the bonding process as the entire fidelity of the parts depending on how efficient the bonding takes place.

Figure 7: Defects (Spaghetti patterns) due to improper bonding [29]

2.4.1 Bonding and Road cooling

Road cooling after the deposition was investigated by Yardimici and Güçeri [19]. They acknowledged the complexity of modeling and focused on the boundary conditions and interaction of the roads. Each road was modeled as a one-dimensional grid block which could be either closed roads or openly ended roads. Their model consisted of the interaction of these blocks with the environment and the adjacent bead. The interaction of the block with the environment was modeled by including a sink term in the governing equation. On the other hand, the interaction of adjacent blocks depends on their position. If the block was on the exterior then it acts as a sink term, however, if it was deposited on

an adjacent block then the neighboring block acted as a source term as it would have a temperature history and transfer the heat to the new block.

$$\rho \frac{\partial q}{\partial t} = k \frac{\partial^2 T}{\partial x^2} - S_c - S_1 \quad (2.1)$$

q =Specific enthalpy

$S_c = \frac{h}{h_{eff}}(T - T_e)$, $S_1 = \frac{k}{w^2}(T - T_{niegh})$

h = convective heat transfer coefficient

h_{eff} = Ratio of road element volume to surface area

T_{niegh}= Temperature of neighboring road

w = Width of the road

2.4.2 Boundary conditions:

Yardimici and Güçeri used multiple evolving grid blocks according to the geometric description. The transient heat transfer analysis was carried out using the finite volume method for the spatial and temporal terms. The transient heat transfer stores the interface temperature history of the moving boundary. Furthermore, they defined a critical bonding temperature which would serve as a threshold of diffusive bonding. The bonding would take place only above the critical temperature T_c and below T_c, the diffusive bonding will be deactivated. Based on this critical temperature a bonding potential may be defined in the following way [19]:

$\Phi = \int_0^t (T - T_c) d\tau$ (2.2)

T= Interface Temperature

T_c = Critical bonding temperature

τ= Integration variable

2.5 Calculation of Bond potential

In this section we, will discuss the calculation of the bond potential, what factors are involved, what research has been done before and we will discuss briefly about calculation of interface temperature using the FEM analysis. Additionally, it also specifies the assumptions made in the process.

2.5.1 Calculation of interface temperature

The calculation of the interface temperature was the major challenge as it involves capturing temperature with respect to time. The following topics explain involve calculation of the interface temperature analytically and numerically using FEM.

2.5.1.1Analytical method

One of the major challenges in the research of FDM is determining the temperature history of the road after deposition. The process is time dependent and has an increasing geometry. A 2D thermal model was presented by Thomas and Rodriguez [20]. They considered the beads to be rectangular for simplicity instead of an oblong shape.

$$T_{ave}(x,y,t) = \mathrm{Te}[1+\sum_{m=1}^{\infty}\sum_{n=1}^{\infty}+a_{mn}\sin(\lambda_m y)+cos(\beta_n x))\times\exp(-\left(\frac{k}{C\rho}\right)^2\left({\lambda_m}^2+{\beta_n}^2\right)t)] \quad (2.3)$$

Where,

$$a_{mn}=\frac{4T_l}{{E_m}^2{F_n}^2\lambda_m\beta_n}\sin(\frac{9\lambda_m H}{2})\sin(\frac{\lambda_m H}{2})\sin(\frac{\beta_n W}{2})$$

$${E_m}^2=\frac{1}{2}(5\mathrm{H}-\sin(\frac{10\lambda_m H}{2\lambda_m})$$

$${F_n}^2=\frac{1}{2}(\mathrm{W}-\sin(\frac{10\lambda_m H\beta_n W}{\beta_n})$$

t= time

C= heat capacity

k= thermal conductivity

ρ= density

Eigenvalues

$$\lambda_m \cot(5\ \lambda_m H) = \frac{-h}{k}$$

and

$$\beta_n \tan(\frac{\beta_n}{k} W) = \frac{-h}{k}$$

The above model neglected the effects of conduction to the build surface and any contact resistance between filaments. The effect of conduction of bed is a crucial as it is predominant in the process according to Bellehumeur [21]

Later, Sun and Bellehumeur observed that the above 2D analysis showed temperature gradients that rapidly become negligible along the width and height of the filament and proposed a lumped capacity model. The simplified 1D governing equation can be given as [22]:

$$\rho CAv\frac{\partial T}{\partial x} = A\frac{\partial\left(\frac{k\partial T}{\partial x}\right)}{\partial x} - hp(T - T_\infty) \quad (2.4)$$

The analytical solution of the above governing equation is:

$$T = T_\infty + (T_o - T_\infty)e^{-mx} \quad (2.5)$$

Where,

$$m = \frac{\sqrt{1 + 4\alpha\beta} - 1}{2\alpha}$$

$$\alpha = \frac{k}{\rho Cv}$$

$$\beta = \frac{hP}{\rho CAv}$$

Equation (2.5) is known for its simplicity and one can estimate the temperature profile along the length of the road. However, it does not consider factors like the bed temperature and considers the temperature to be uniform along the cross-section.

2.5.1.2 Finite Element method:

Finite element method (FEM) was used to calculate the interface temperature (T). The FEM analysis was done in COMSOL Multiphysics version 5.2a under the time-dependent 'Heat transfer in solids' section. Time-dependent heat transfer governing equation used in the software is [COMSOL 5.2a©]:

$$\rho Cp \frac{\partial T}{\partial t} = \nabla(k\nabla T) + Q \qquad (2.6)$$

The above equation is a transient heat transfer equation where ρ, Cp and k depend on the material [24]. The above heat transfer equation accepts two types of boundary conditions: specified temperature and specified heat flux. The specified temperature condition is a surface phenomenon where you can specify the temperature T_0 at the boundary. On the other hand, inward heat flux is specified by the equation [30]:

$$-nq = q_0 \qquad (2.7)$$

Where:

q is the conductive heat flux vector (SI unit: W/m^2), q = $-k\nabla T$.

n is the normal vector on the boundary, q_0 is the inward heat flux (SI unit: W/m^2), normal to the boundary. The inward heat flux, q_0, is a sum of contributions from different heat transfer processes (for our case, convection). If q_0= 0 then the boundary would be called as a thermally insulated boundary.

For convection:

$$q_0 = h \cdot (T_{ext} - T) \quad (2.8)$$

Where T_{ext} is the ambient temperature h, represents the heat transfer coefficient, which is all the physics occurring between the boundary and ambient air [29]. 'u'(m/s^2)- is the velocity field defined by the Translational Motion sub-node when parts of the model are moving in the material frame. In our case we consider the value of u to be zero. Finally, Q (SI unit: W/m^3) is additional heat source (or sink). Since our analysis does not have any additional heat source the value of Q is also zero [24]

The interface temperature in FEM model will depend upon recreating the boundary conditions required for the analysis. COMSOL 5.2a has numerous features to capture the same. The attempt is also to incorporate the conduction with the bed which is not present in the analytical model. The process is explained in detail in chapter 3.

2.5.2 Critical temperature:

There has been no specific literature which focusses the critical temperature. Even in the analysis done by Yardimici, the critical temperature has been selected as a certain value. Hence, due to the lack of information, the critical temperature has been estimated in the following analysis. It hence becomes imperative to investigate regarding the same.

Chapter 3 Methodology

The methodology for calculating the bond potential is discussed in this section. The main focus in this section is the calculation of interface temperature. Fig- showcases the process followed to calculate the interface temperature. This process has been adopted to compare the results with the analytical solution mentioned above. Secondly, it includes a proposed 3D model to obtain the interaction of beads which is not limited to the 1D equation of Sun and Belleheumer [22], instead, it showcases the interaction with surroundings as well. Thirdly, it lays out a method to compile an extensive amount of data required for calculating the bond potential. Finally, it describes the experimental setups required to compare the proposed FEM model.

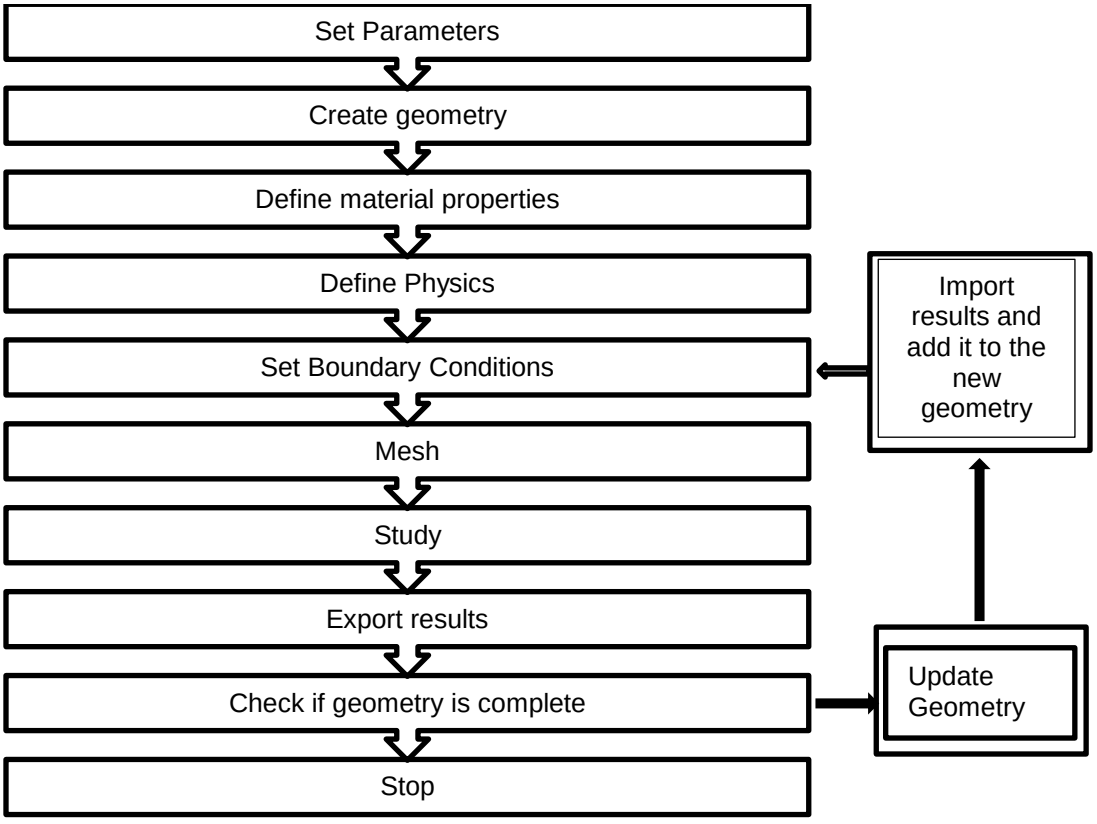

Figure 8: The model workflow to caluclate interface temperature

3.1 Model Setup

The most challenging part of this thesis was to incorporate a moving boundary or a changing geometry. The focus entirely on the boundary conditions of the heat transfer phenomenon. However, incorporating a moving boundary was still a challenge. Thus, it was decided that there could be multiple heat transfer analyses rather than a single analysis. The approach was to carry out an analysis, store its result, manually change the geometry for the next analysis, import the previously stored result, update the boundary conditions keep repeating this process for a given geometry till it is complete. Thus, the analysis could be performed by changing the geometry and obtain a time history of the interface temperatures, which would be later used in the bond potential calculation.

The following topics explain the process of the model set up in detail:

3.1.1 Set parameters:

Before carrying out the analysis, we needed to set certain parameters. These parameters remain constant throughout. The value of these parameters remained constant during the analysis and have been set globally. The reason for this is that, if there were any changes in the process we can incorporate them at this step rather than changing each and every parameter at different stages of analysis. The parameters for the same are:

1. Liquefier Temperature (T_l): This temperature corresponds to the extruder temperature mentioned for ABS. The extruder temperature is taken to be 230^{o}C [25] as the printing of the specimen was done in Polyprinter. However, there are many papers which consider the temperature to be 270^{o}C [22,28]. In the following analysis, where ABS has been considered. Hence, the temperature was set up to be 230^{o}C.

2. Environmental Temperature (T_e): The environmental temperature is a variable. As the two tensile specimens were printed in PolyPrinter, they were enclosed in a large casing. Thus, the temperature was assumed to be 50^{o}C.
3. Bed Temperature (T_{bed}): The bed temperature was taken to be 110^{o}C for analysis of ABS according to the conditions specified in PolyPrinter [25]. However, for the experimental analysis where the material was PLA, it was taken to be 60^{o}C.
4. Geometrical parameters: length (l), breadth (b) and height (ht): the height corresponds to the layer height. The length and the breadth were assumed to correspond to the layer thickness.
5. The speed of the printer was 50 mm/s. This is the speed of the gantry which will determine the duration of the analysis

3.1.2 Create geometry

Yardimici considered multiple evolving grids and hence rectangular blocks were considered with the dimensions of 0.35 mm as length (l) and breadth (w) and 0.25 as height (ht). For experimental analysis the dimensions of 0.355 mm as length (l), 0.4 as breadth (w) and 0.4 as height (ht)

3.1.3 Define material properties:

The material properties were applied to the entire domain. Over the course of the thesis the analysis was carried out in two materials; ABS for tensile specimens and PLA for the comparing with the experimental data. The material properties required for the analysis were as follows: Density, specific heat and thermal conductivity.

Table 2: Material properties used for the analysis

Sr no.	Property	Values	
		ABS	PLA
1	Density	1050 kg/m^3	1300 kg/m^3
2	Specific heat	2080 J/kgK	1800 J/kgK
3	Thermal conductivity	0.177 W/mK	2 W/mK

3.1.4 Define Physics

This section discusses the type of analysis carried out and the boundary conditions that were applied. We have already discussed the theory of the time-dependent 'Heat transfer in solids' in section 2.5.2. There are three main boundary conditions and two types of initial conditions applied in the analysis. They are as follows:

3.1.4.1 Initial Value (Initial Condition):

The initial value is a node that adds an initial condition for a transient analysis. It is applied to the entire domain; In this case, the domains are the evolving blocks. COMSOL Multiphysics has a feature where this node can be applied to multiple domains. There are two initial values applied during the analysis. The first initial value is the extruder temperature (T_I). (Refer Figure-9).

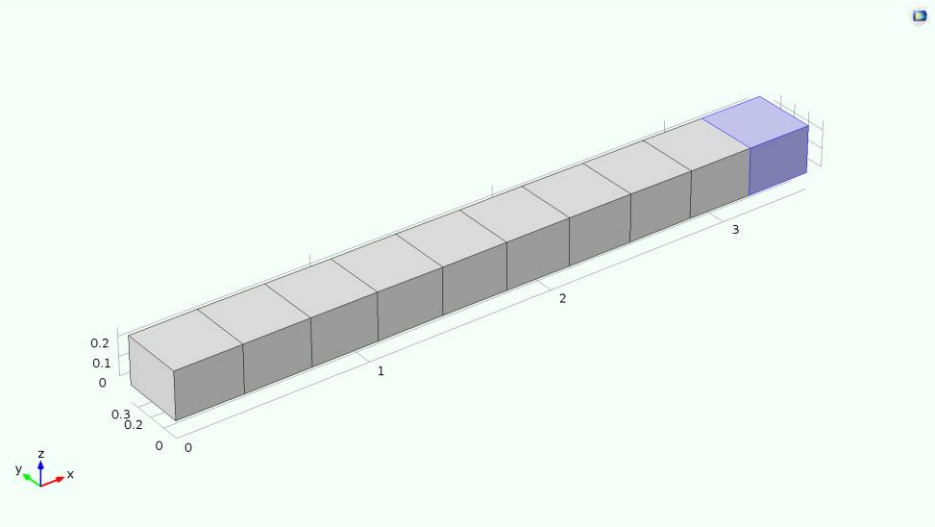

Figure 9: Extruder temperature T_I applied to the new grid.

After the analysis was carried out the resultant temperatures were exported to a spreadsheet with the temperature values along each node (x, y and z coordinates).

These values were then imported by an interpolation function which interpolates this stored temperature and serves as an initial condition for the previously analyzed blocks.

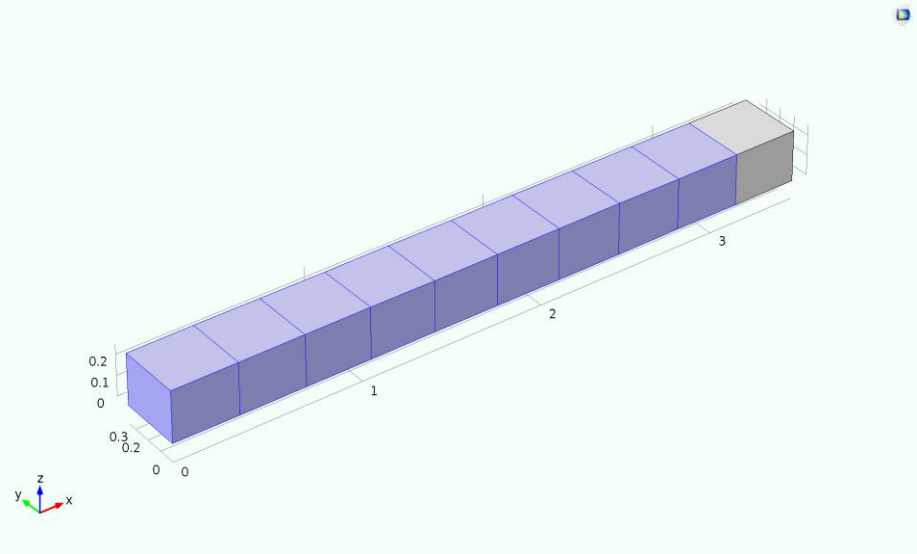

Figure 10: The initial values using interpolation function (int1) as input

3.1.4.2 Convection:

Convection is the most dominant boundary condition and is applied on 5 surfaces of the block, except the bottom. Convection is applied in form of a heat flux in COMSOL Multiphysics. There are two important inputs to set up convection: The heat transfer coefficient (h) and the ambient temperature (T_e).

Initial analysis was carried out with a user-defined value of h. After comparison with the experimental analysis, the heat transfer coefficient went through several revisions. Finally, another feature in COMSOL Multiphysics was applied. Depending upon the geometry and the application, COMSOL Multiphysics has an inbuilt feature where a convective correlation can be applied. The convective correlation is an empirical relationship, which is developed for common geometries [26]. According to the

geometry of the rectangular blocks, a vertical plate upside was selected. The input required was the plate diameter, which is the ratio of area and to the perimeter of the plate. The ambient pressure selected was 1 bar and the ambient temperature reflected T_e.

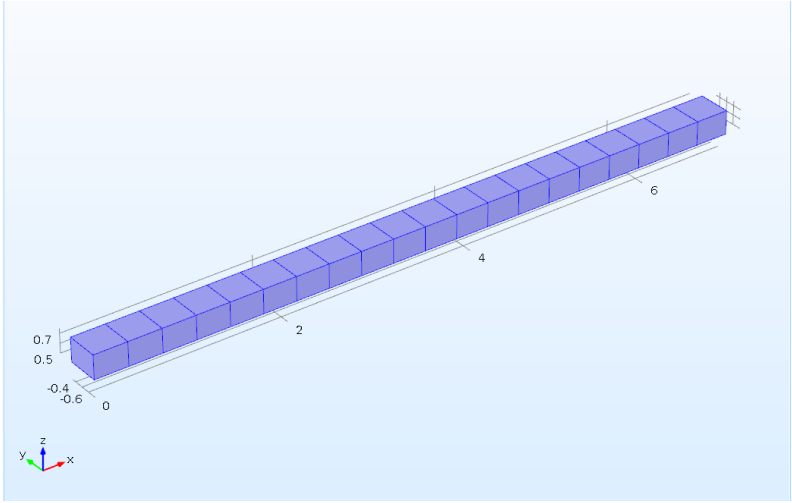

Figure 11: Convection boundary condition applied on 5 sides of the blocks

3.1.4.3 Bottom Surface:

For the bottom surface, it was imperative to incorporate the conduction phenomenon. There were several revisions made to the analysis based on capturing the appropriate boundary condition for the bottom surface. Through various analyses and comparisons with the experimental result, it was found that, if the extruded bead is analyzed at the bed, then it becomes imperative to model the bed(substrate) and capture its interaction with the bottom layer. The bed when exposed to a certain temperature Furthermore, the bottom layer of the block will be in contact with a thermally insulated bed with a constant bed temperature applied at the bottom of the bed geometry.

While investigating appropriate boundary condition in COMSOL Multiphysics, it was observed that the 'Temperature' boundary condition when applied will keep that particular surface at the same temperature. Hence, it was applied on the bottom surface of the modeled bed and not on the surface of the bed.

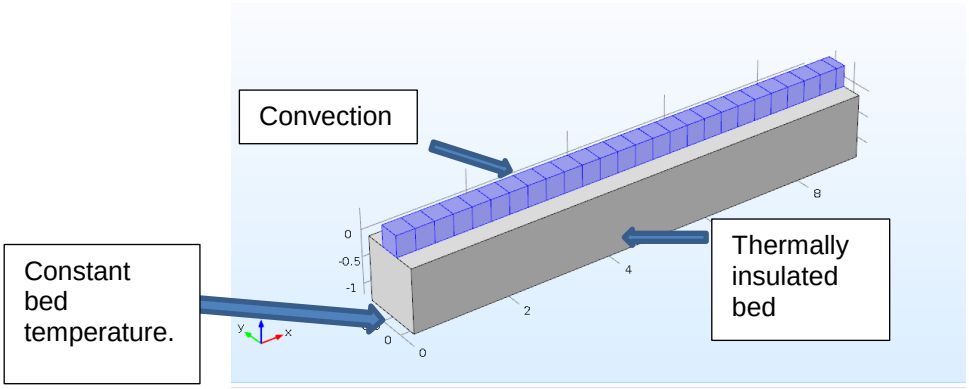

Figure 12: Boundary condition considering experimental data

For the analysis of the tensile specimen, the extruded beads are at a higher region. Due to the low thermal conductivity of polymers, the interaction of bed is lower than the interaction the bottom layer.

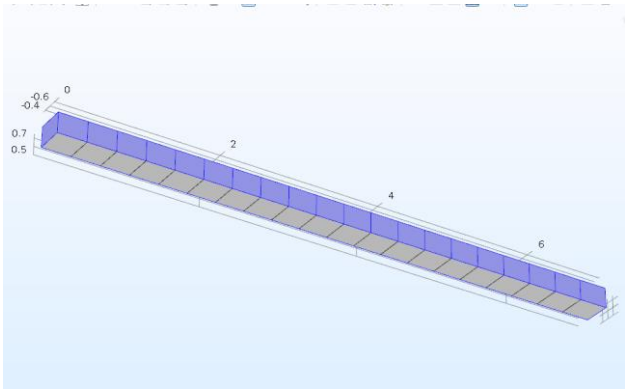

Figure 13: Bottom section being thermally insulated for layers higher than the bed

Over a period of time the layers higher than the bed to reach the bed temperature and hence, a revised model was proposed where a base layer was initially considered at bed temperature and then the analysis was carried out between top two

layers. Here the bottom layer was kept insulated as shown in Figure 9. The reason for this is that the base layer will be exposed to the bed temperature and the heat transfer has already reached its saturation state.

3.1.5 Interpolation function

There are many functions available in COMSOL which can be added globally or locally. An Interpolation function is defined by a set of values of the function in discrete points. The temperature values after every analysis are stored in the nodes of the mesh along the x, y, and z coordinate. These temperature values are exported in form of a grid or a spreadsheet according to their corresponding location resulting into a table with temperature as a function and spatial coordinates as arguments. COMSOL 5.2 a can import data of the function up to 3 arguments (Temperature at x, y, and z-co-ordinates. These functions can later be added into the model as an initial value, thereby storing the temperature history and allowing us to recreate the multiple evolving blocks for our analysis.

3.1.6 Mesh

To obtain optimal mesh size, several analyses were done at the beginning with different mesh size. Initially, all the –analyses were done in physics-controlled meshing in the normal and the extremely fine feature. Even though the results were closed due to the changing geometry, the mesh density was inconsistent. Hence a user-defined mesh was chosen. The inputs of the mesh density are mentioned below and the comparison with normal mesh density and the extremely fine feature has been given below.

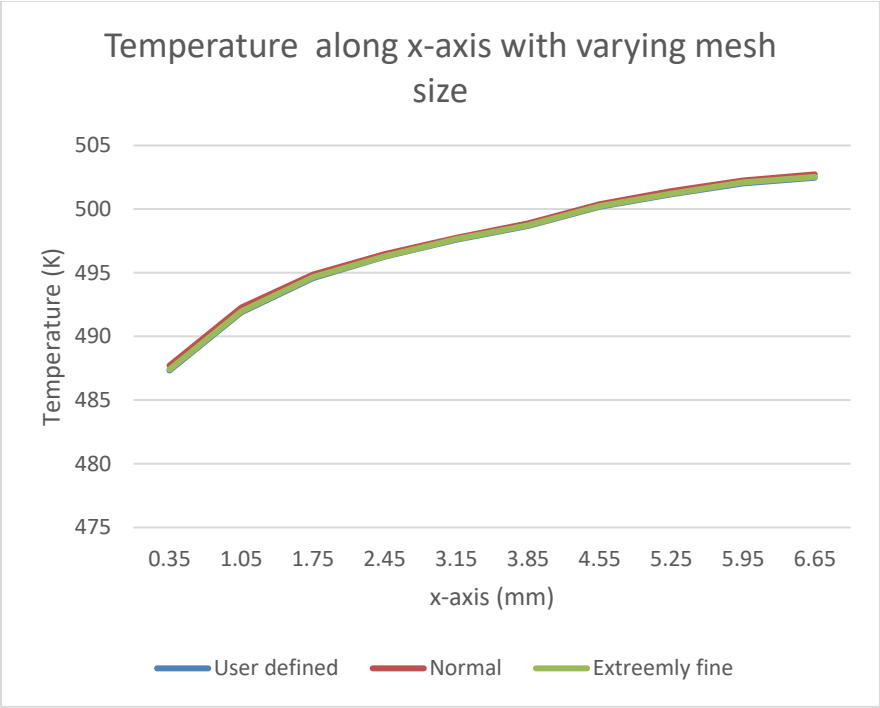

Figure 14: Comparison of Temperature with different mesh sizes

3.1.7 Study

This section covers the time period for which the analysis was carried out. Each element is 0.35 mm in length. The speed of the gantry is 50 mm/s. Hence the time of analysis for each block was the ratio of the length (distance) to the speed of the gantry (speed), which is 0.007 s. The time step for the analysis was selected as 0.001 sec.

3.2 Model parameters

In order to perform a parametric study with respect to geometry and heat transfer coefficient, the analysis was carried out between two beads of different length; 7 mm and 14 mm. Initially, there were only 2 layers along the length with common width and thickness. Furthermore, the analysis between the two specimens was done twice; Once with h=50 W/m^2K and the second time with h=100W/m^2K. Later, the experimental analysis was performed which led to further revisions in the analysis. The final analysis

was carried out using a convection correlation and included a base layer along with the 7 mm and 14 mm specimens.

3.3 Compilation of results:

The analysis consisted of multiple evolving grids. Hence, the results had to export numerous times. A typical export comprised of 3 types of data. Firstly, the temperature across each node of the mesh which would be later used to import in the next analysis. Secondly, the surface temperature with respect to time at any particular value of x-axis. Thirdly the surface temperature between the top and the bottom layer gather the interface temperature which would be later used to calculate the bond potential.

After compiling the temperature values for the bond potential, there were further edits to be done. Firstly, clear out the temperature values where contact has not occurred. Thus, the first few rows of every new column imported were to be manually deleted to a point where the top layer came in contact with the bottom layer. Secondly, all the values needed to be subtracted by the critical temperature and finally each value needed to be multiplied by the time step. Additionally, there were certain values where the difference with the critical temperature leads to a negative value. This, in turn, would bring erroneous results while integrating along the length. Hence, these values were to be made zero.

The final 7mm specimen consisted of 160 files containing results and the 14 mm file has 320 files. The analysis itself was time-consuming as the complexity of the part increased. Furthermore, gathering results after the analysis manually carrying out the above edits was indeed an industrious task. Hence, a MATLAB code was written to

compile the data and carry out the above tasks. This considerably reduced time and efficiently carried out all the calculations for bond potential.

3.4 Experimental analysis:

In order to validate the process followed above, it was compared with experimental analysis. The experimental setup was done in 'Microscale Thermophysics Lab' at the University of Texas at Arlington. The experiments were carried out under the supervision of Dr. Ankur Jain and Mr. Darshan Ravoori. The experiments were carried out in Anet autoleveling A8 3D printer and the temperature measurements were carried out using an infrared camera A6700 SC FLIR.

The parameters for the experiments are explained in the result's section 4.4

Chapter 4

Results

4.1 Analytical Model

The analytical equation (2.5) was incorporated in COMSOL Multiphysics to observe and compare the behavior with the proposed model which consists of evolving grids. The parameters for the same is mentioned below:

Table 3 Parameters for Analytical modeling

Sr no.	Parameters	Values
1	Extruder temperature (T_I)	230^{o}C
2	Environment Temperature (Te)	50oC
3	m (geometrical parameter)	6.038[1/m]
4	Length	7 mm
5	Width	0.35 mm
6	Height (Layer thickness)	0.25 mm
7	Convection	All sides(h=50W/m^{2}K)

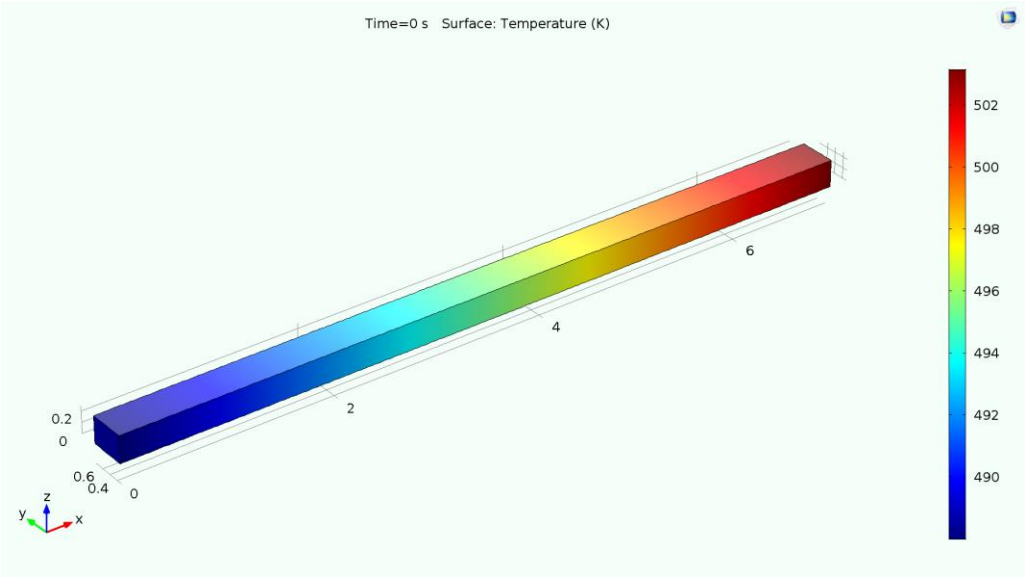

Figure 15 Temperature profile of 1D equation applied to the specimen.

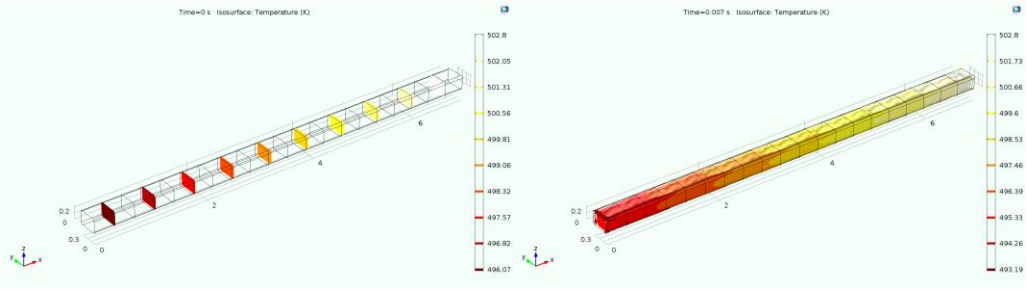

(a) (b)

Figure 16: Isothermal contours of the analytical model. (a) is at time 0 s and (b) is at 0.007 s

From the above results, it is clear that the analytical model does not consider convection. This can be seen in Figure 16 (a), where the isothermal contours are consistent at 0 s. This is because the equation is one dimensional and is consistent along y and z-axes.

4.2 FEM Model and comparison with analytical model

The FEM model as explained before has multiple evolving grid blocks analyzed successively by storing results for the next analysis and importing them using interpolation function. The FEM model also considers interaction (conduction) with the lower bead or the bed. In the following case, interaction with the lower bead is considered instead of the bed and the dimensions are consistent with the analytical model. This is done by carrying out analysis of 20 blocks along the x-axis.

Table 4: Parameters for the FEM model

Sr no.	Parameters	Values
1	Extruder temperature (T_l)	230^{o}C
2	Environment Temperature (Te)	50^{o}C
3	m (geometrical parameter)	N/A
4	Length	0.35 x 20
5	Width	0.35 mm
6	Height (Layer thickness)	0.25 mm

Table 4.2 -*Continued*

7	Convection	5 sides(h=50W/m^{2}K)
8	Bottom surface	Thermally insulated

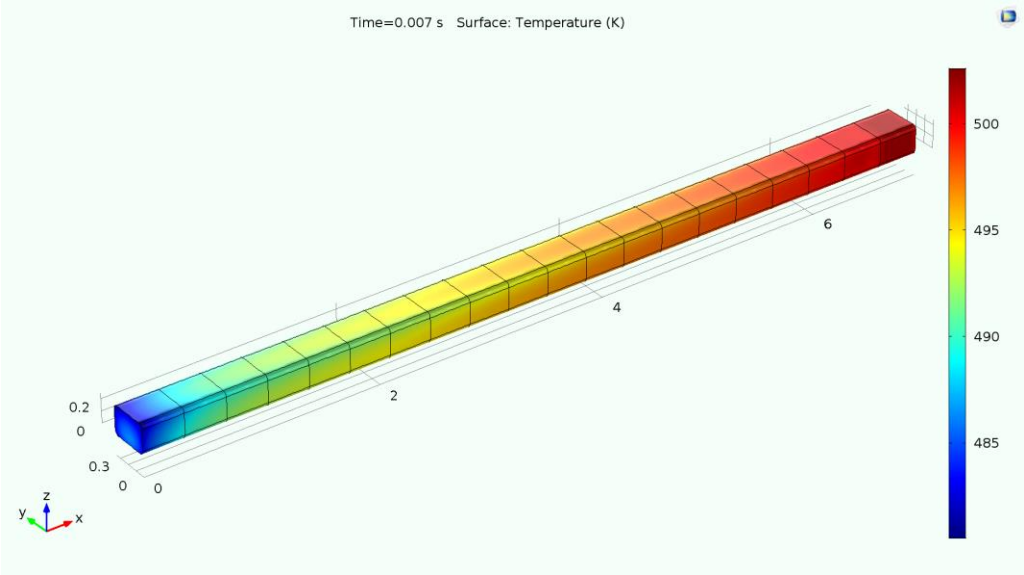

Figure 17: Temperature profile of the proposed model

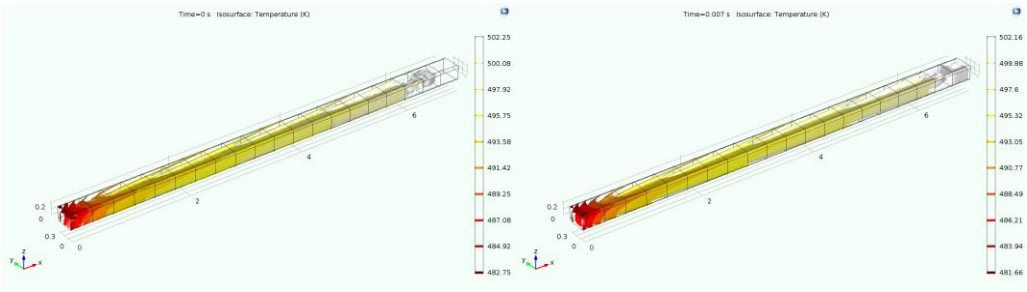

(a) (b)

Figure 18: Isothermal contours of the FEM model.17(a) is taken at 0 s and 17(b) at 0.007 s

Comparing the isothermal contours of the analytical model in Figure 15 with that of the FEM model in Figure 17, it is clear that the effect of convection occurs right from the first block in the FEM analysis and is not considered for the analytical equation. This is because the analytical equation at 0 s represents a temperature profile which has not been affected by convection before.

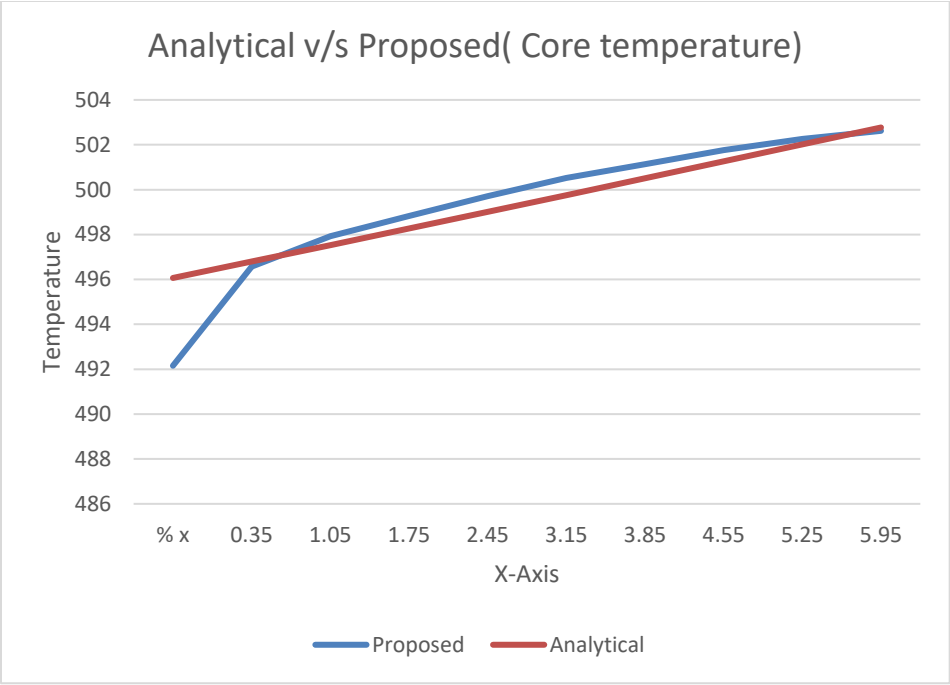

Figure 19: Comparison of temperature at the core of the extruded bead.

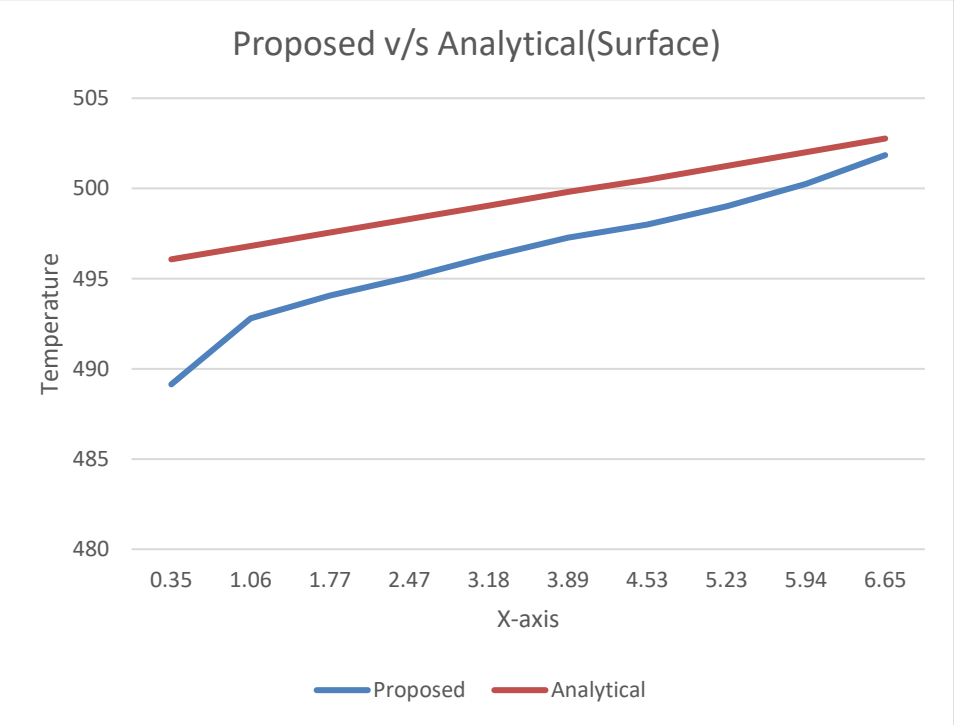

Figure 20: Comparison of temperature at the surface of the extruded bead.

From Figure 18, we can clearly see that the temperature at the core region is almost similar but not at the surface. This is because the convection takes place at the surface. As discussed earlier, the analytical equation does not consider the convection which starts immediately after the deposition of the bead.

Comparing both the results our next approach was to explore the thermal interaction with multiple layers using the proposed FEM model. Thus, the interface temperature for the bond potential calculation was carried out using the FEM model.

4.3 Bond Potential for tensile specimens

Two tensile specimens of different lengths (7 mm and 14 mm) were analyzed. The geometry consisted of 20 blocks which made up a 7 mm bead along the length and similarly 40 blocks made up a 14 mm specimen. All the other parameters were kept same as Table:4. It is important to note that the heat transfer coefficient was kept at h=50 W/m^2K for the first group of analyses and later the heat transfer coefficient was modified to 100 W/m^2K.

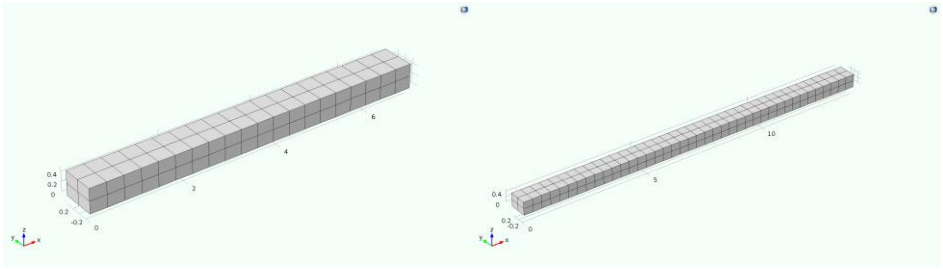

(a) (b)

Figure 21: The geometry using multiple grid blocks. 20(a) is 7 mm and 20(b) is 14 mm

The mesh density was kept common for both the analyses. The mesh density parameters are shown in Table 5:

Table 5 User-defined mesh parameters

Sr no	Parameter	Value
1	Maximum element size	0.1 mm
2	Minimum element size	0.07 mm
3	Maximum element growth rate	1.3
4	Curve factor	0.3
5	Resolution of the narrow regions	0.85

The bond potential was calculated at the interface between the two layers (top and the bottom). Interface temperature (T) was calculated at the midpoint of the width (0.175mm) and at a height of 0.25 mm. The results were extracted in form of 80 spreadsheets for 7 mm specimen and 160 spreadsheets for 14 mm specimen. Each result was compiled using MATLAB which is explained in section 3.3.

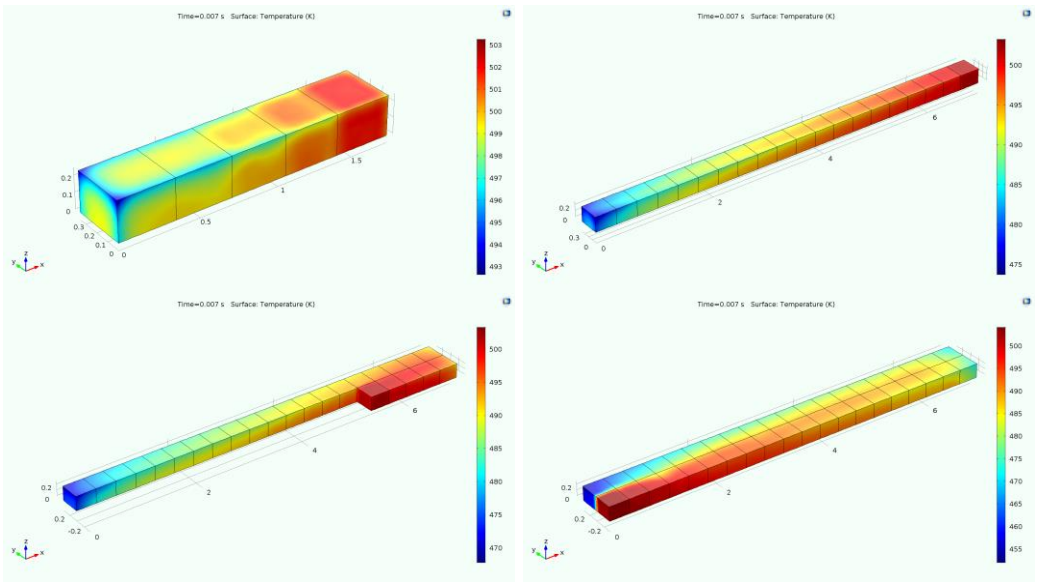

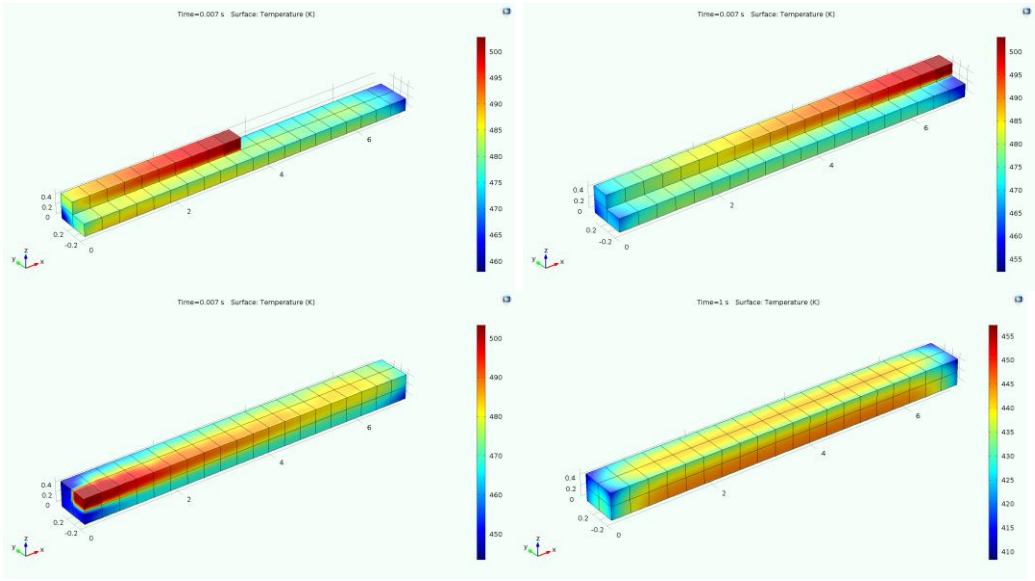

Figure 22 The temperature profile of multiple evolving grids from time (0 to 1.56 s)

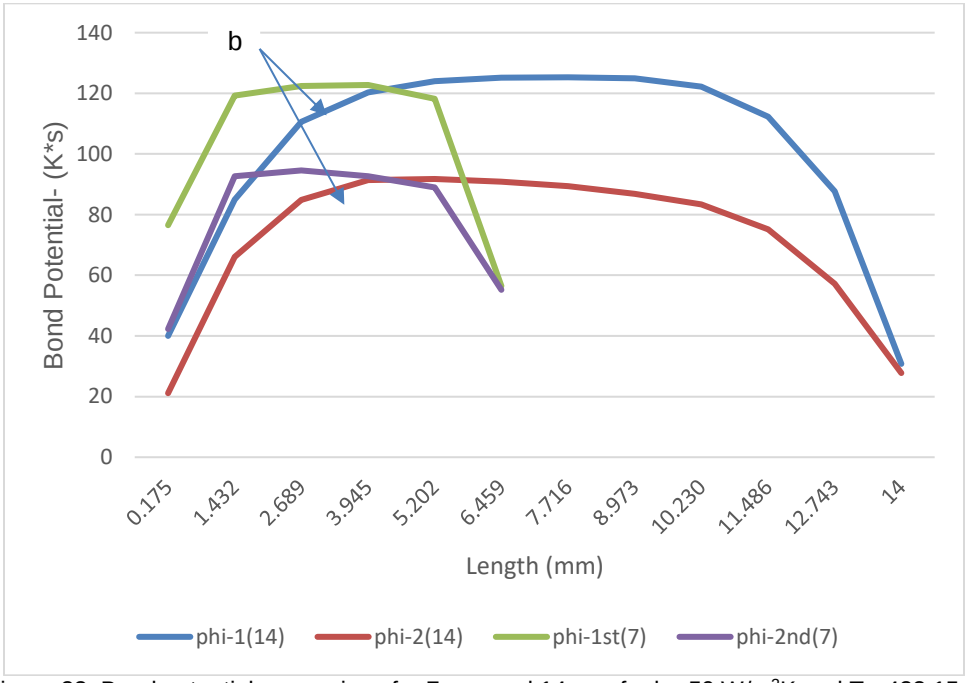

Figure 23: Bond potential comparison for 7 mm and 14 mm for h= 50 W/m^{2}K and T_c=423.15 K

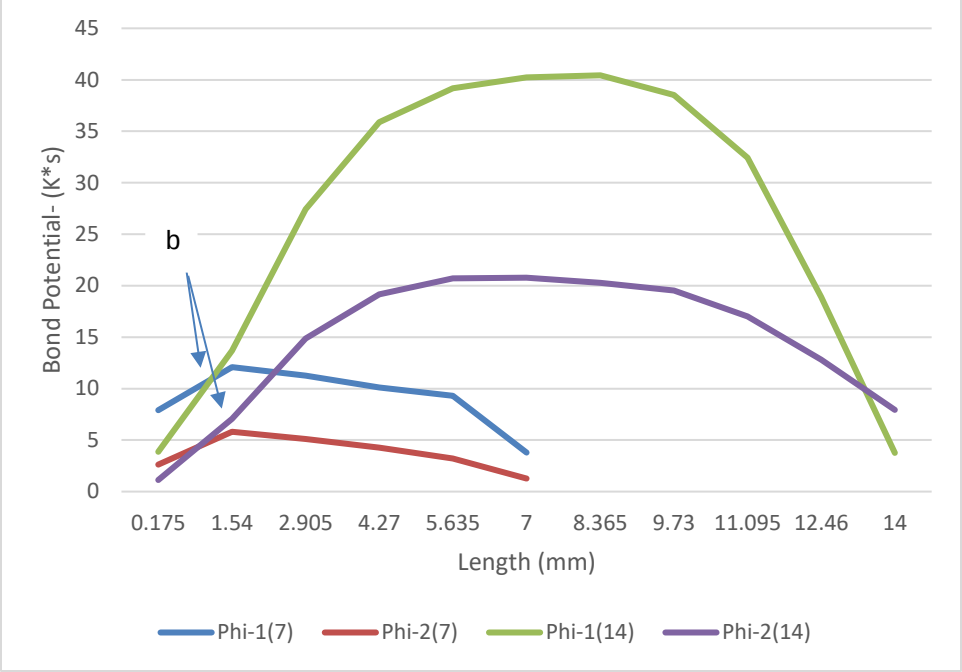

Figure 24: Bond potential comparison for 7 mm and 14 mm for h= 100 W/m^{2}K and Tc = 423.15 K

From figure 22 and 23 the following observations were made:

1. The value of bond potential is low at the endpoints of the length as compared to the mid-section. This is because the cooling of the bead starts from the endpoints and propagates towards the center (Figure 25). This suggests that the endpoints along the length have lesser time to bond as compared to the midsection.

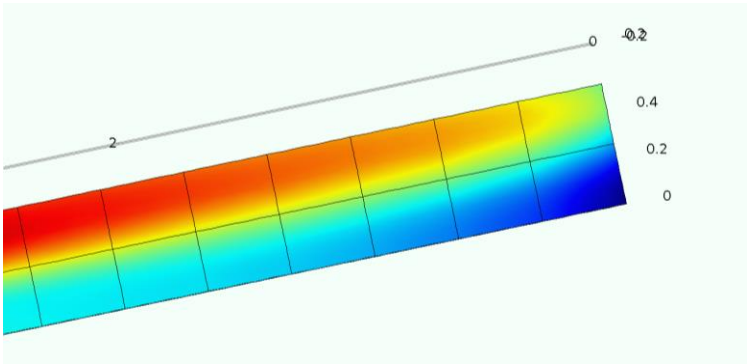

Figure 25: Cooling initiated from the endpoints of the specimen.

2. The bond potential is highly sensitive to the heat transfer coefficient. Lower heat transfer coefficient (h=50 W/m^{2}K) leads to a higher value of bond potential (Figure 22) as compared to the specimens which had a higher value of heat transfer coefficient (h=100 W/m^{2}K).

   This is because the higher heat transfer coefficient controls the convection and causes higher heat transfer rate, due to which the overall bonding time is less. Lower heat transfer coefficient causes a lower heat transfer rate. Thus, for lower heat transfer coefficient we have a longer temperature history, which provides more time for the layers to bond.

3. Another observation related to heat transfer coefficient was; for higher heat transfer coefficient the common value of the bond potential for both the specimens corresponds to lower value of the bond potential (point 'b' in Figure 23), which is the exterior end. On the other hand, for lower heat transfer coefficient, the bond potential for both the specimens corresponds to the higher value (point 'a' in figure 22), which is the midsection of the specimens.

4.4 Experimental model:

Experimental analysis was imperative to validate the above method. The methodology for the experiments is explained in chapter 3.4. The experimental analysis data was provided by 'Microscale Thermophysics Lab' with different parameters and a different FDM 3D printer. The updated parameters are given in Table 6.

Table 6: Parameters for the experimental analysis

Printing parameters	Values
Layer thickness	0.2mm
Extruder thickness	0.4mm
Length of the bead	6.7
Extruder speed	1.93mm/s

The model was run for PLA as the material. The material properties of PLA are mentioned in Table-2: Heat transfer coefficient was not provided and hence the model was run at a heat transfer coefficient of 50 W/m^{2}K. Initial FEM model results showcased a h difference in the temperature values.

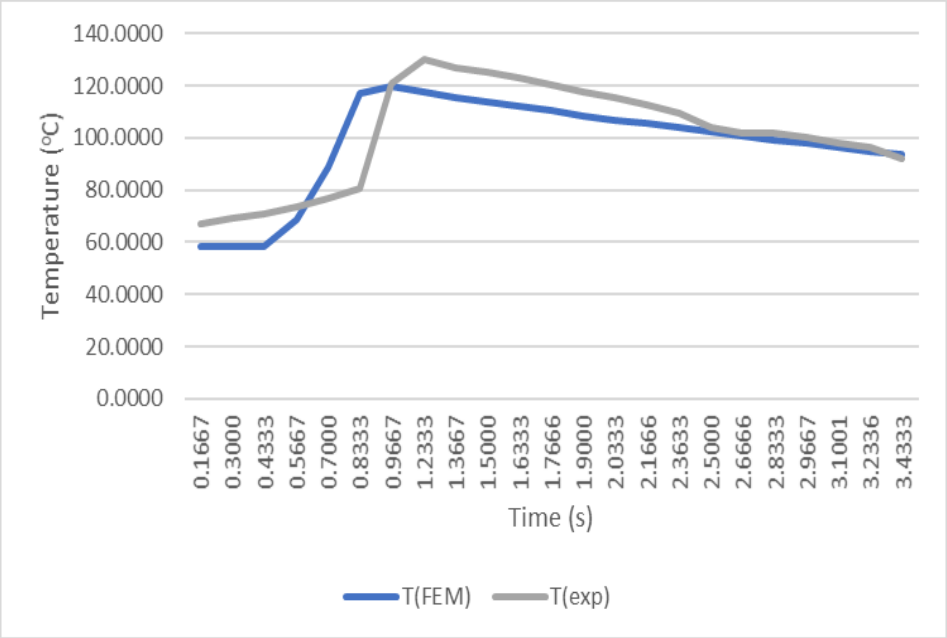

Figure 26: Temperature comparison between FEM and experimental data

The temperature difference led us to believe that the heat transfer coefficient should be taken as a lower value. Hence the analysis was repeated with h=20 W/m2K. Another modification done to the analysis was to carry out the analysis at a time step equal to the time step at which the experimental data was extracted.

The results for h=20 are:

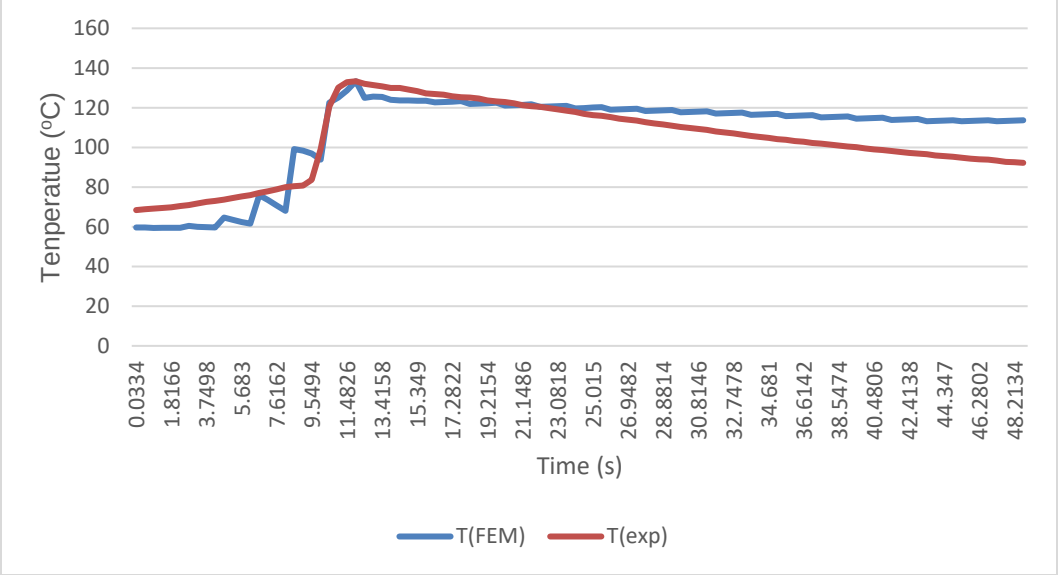

Figure 27: Interface temperature comparison of experimental data with FEM data at x=2.6

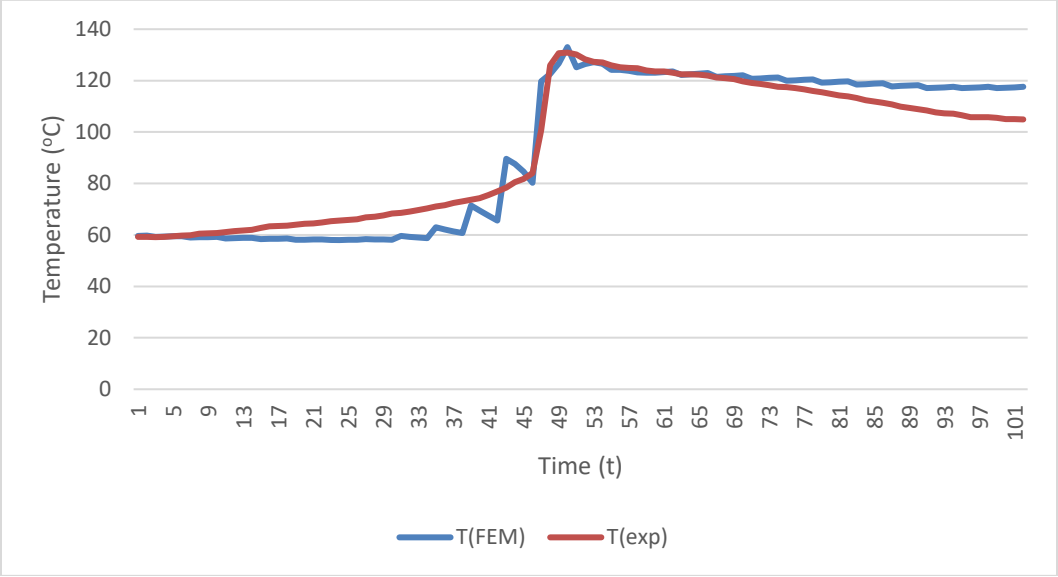

Figure 28 Interface temperature comparison of experimental data with FEM data at x=4.75

The above values extracted show similar peak temperatures, however, the temperature values after the contact don't come into agreement. Low heat transfer coefficient causes slower heat transfer rate and hence the above relation would not be

accurate. The above values are the interaction between the top and the bottom layer. However, the results at the bottom layer led to significant changes in the future analyses.

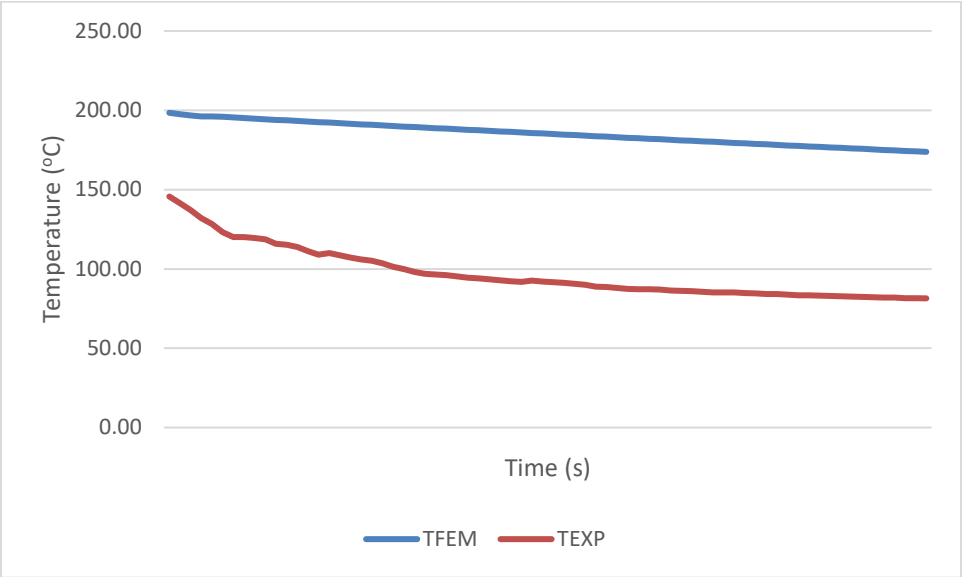

Figure 29: Interface temperature comparison of experimental data with FEM data of the bottom layer

The above figure shows difference between the experimental and FEM analysis. This is due to the bed of the 3D printer, which has not been modeled. The interaction of the bed needs to be taken into consideration and hence the temperature of the FEM model is erroneous for the bottom layer.

The experimental analysis showcased the importance of modeling the bed and also the appropriate heat transfer coefficient. There were several attempts to come up with the appropriate heat transfer coefficient. Unfortunately, it was not successful. Hence, the convection correlation feature in COMSOL Multiphysics was applied to the FEM model. The theory about the same is explained in chapter *3.1.4.2*. Another addition while an investigation of the experimental data was the effect of the nozzle on the interface temperature. It was observed that the nozzle transferred extra heat to the bead. This

phenomenon was captured by Mr. Darshan Ravoori when a dry run of the nozzle (without filament) was made to pass through the bed. The IR camera captured a temperature of 20^{o}C-40^{o}C along the bed. Hence, there is a possibility that the interface temperature captured by the experiments will always be higher than the FEM model or any analytical model [27].

The final FEM analysis to compare the experiments consisted of partial modeling of the bed, due to lack of computational power and use of convective correlation where a 'plate being upside' feature was used.

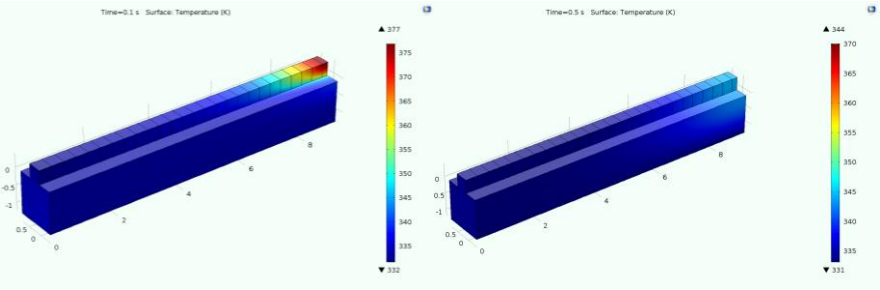

(a) (b)

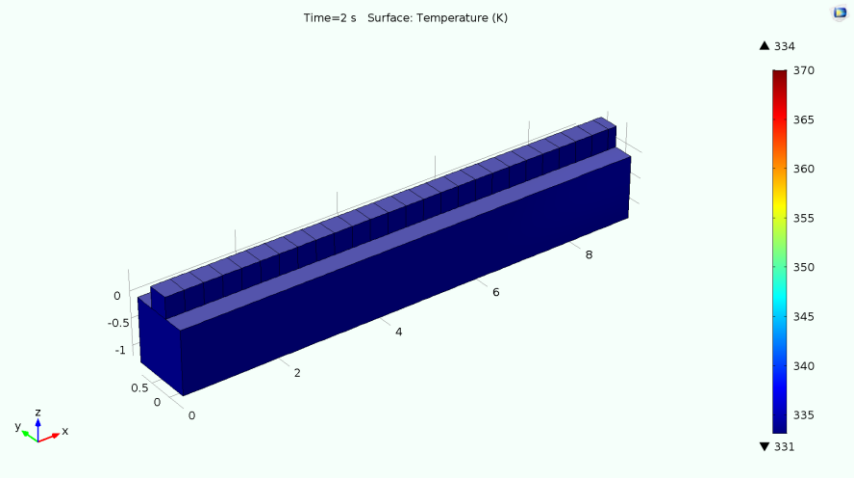

(c)

Figure 30: Figure (a) represents the analysis at 0.1 s. (b) represents an analysis at 0.5 s. (c) represents analysis at 2 s

The results of the same are:

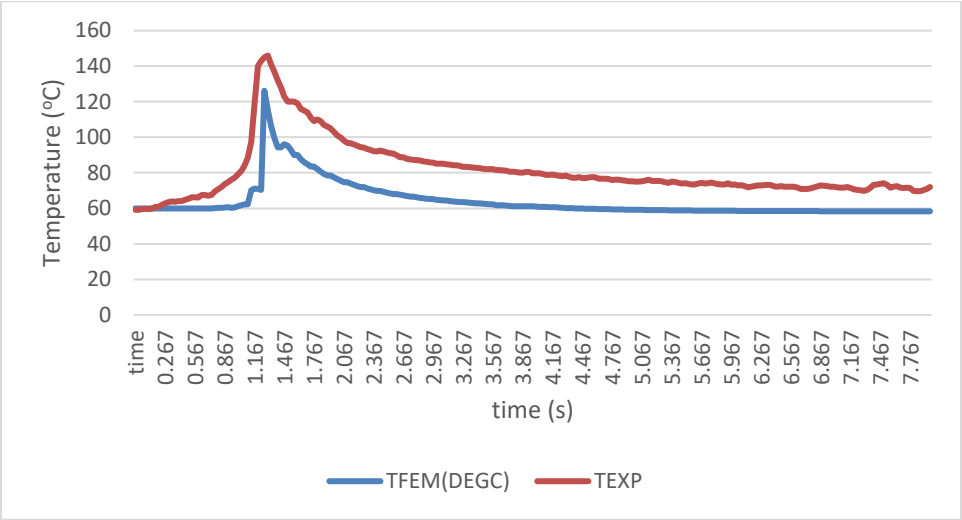

Figure 31: Interface temperature comparison of experimental data with FEM data at x=2.6

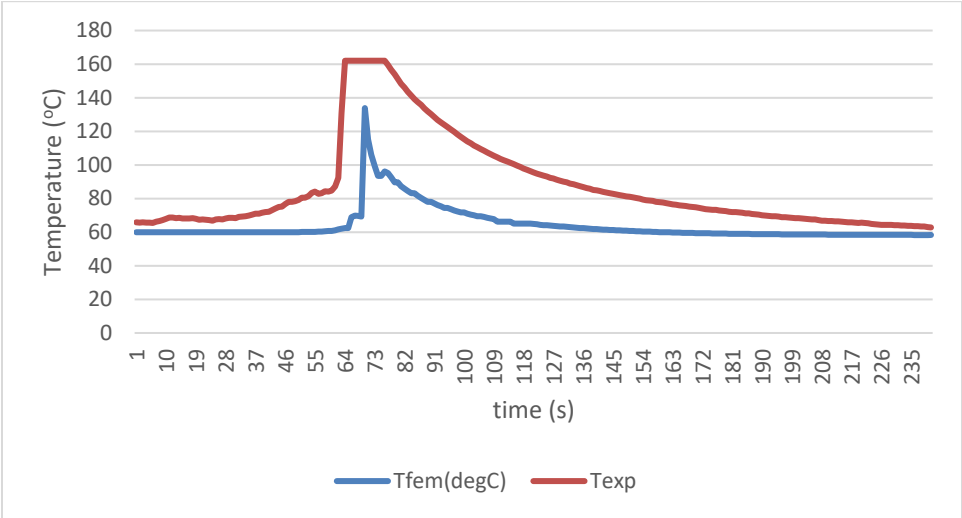

Figure 32: Interface temperature comparison of experimental data with FEM data at x=4.75

It can be observed from Figure 28 that the peak temperature of the FEM model is 12°C below the experimental model. Furthermore, the temperature follows a parallel trend after contact unlike Figure 25 and 26 where the cooling is slow. The reason as a constant temperature at 160°C is because of the limitation of the IR camera. The

temperature of the surface at those points were out of range of the IR camera (above 160^{o}C) and hence figure 29 doesn't follow a parallel trend.

There needs to be a further investigation of different materials and specimens to validate the FEM and experimental data.

4.5 Revised model:

Contrary to the experimental model which was carried out on a bed, the analysis of the tensile specimens was to be carried out at a region higher than the bed. One of the most important observations from the experimental analysis was that the interface temperature of the bead in contact with the bed cools down to the bed temperature. However, the surface higher than the contact region cools down not more than 3^{o}C to the bed(Refer Fig-30 c).

. As there was no consistency as to how low the temperature drops, a base layer of bed temperature of Polyprinter(110^{o}C) was added to the analysis.

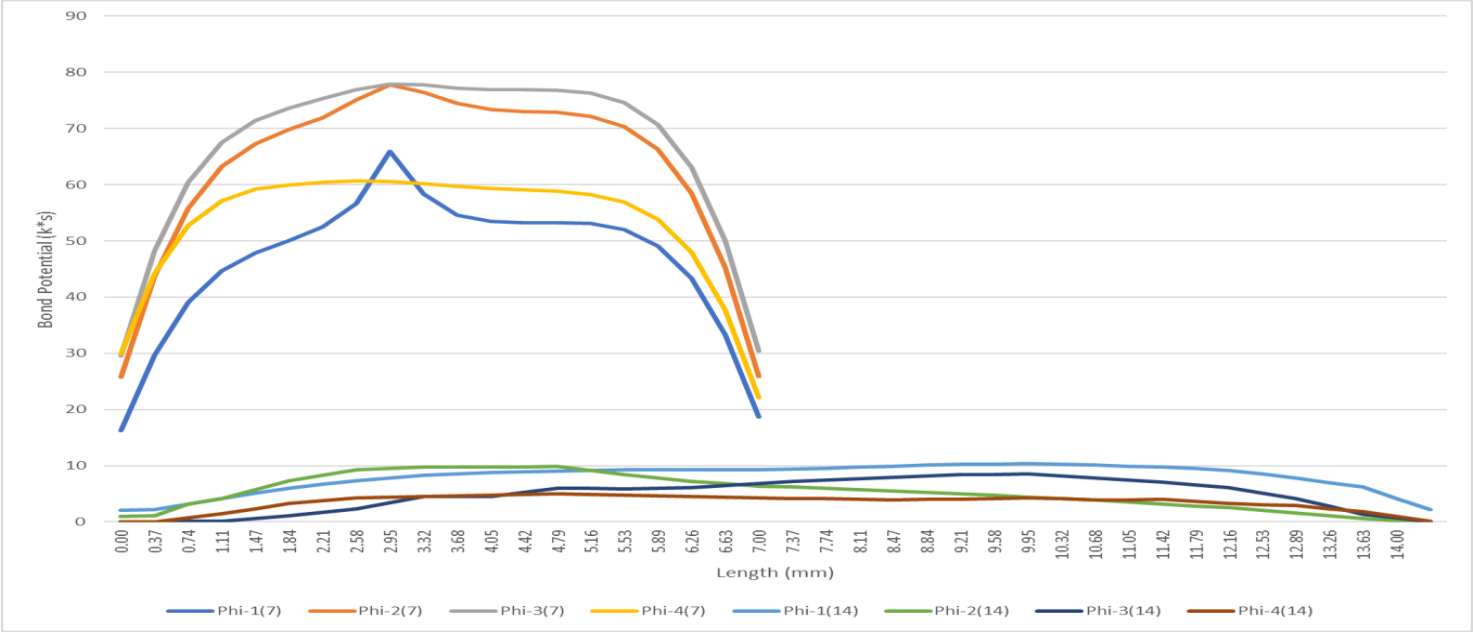

Figure 33: The comparison of bond potential for 14 mm and 7 mm specimen

Additionally, the analysis was carried out using the convective correlation and instead of two bead an addition to four beads across two layers was performed to understand the bond potential better. The results of the same are in Figure 33-35:

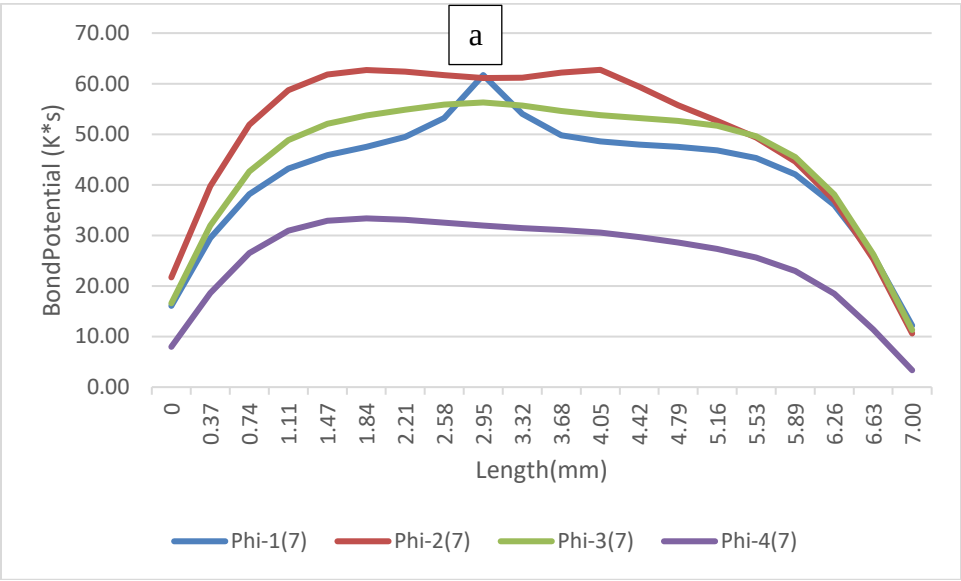

Figure 34: Bond potential for 7 mm specimen

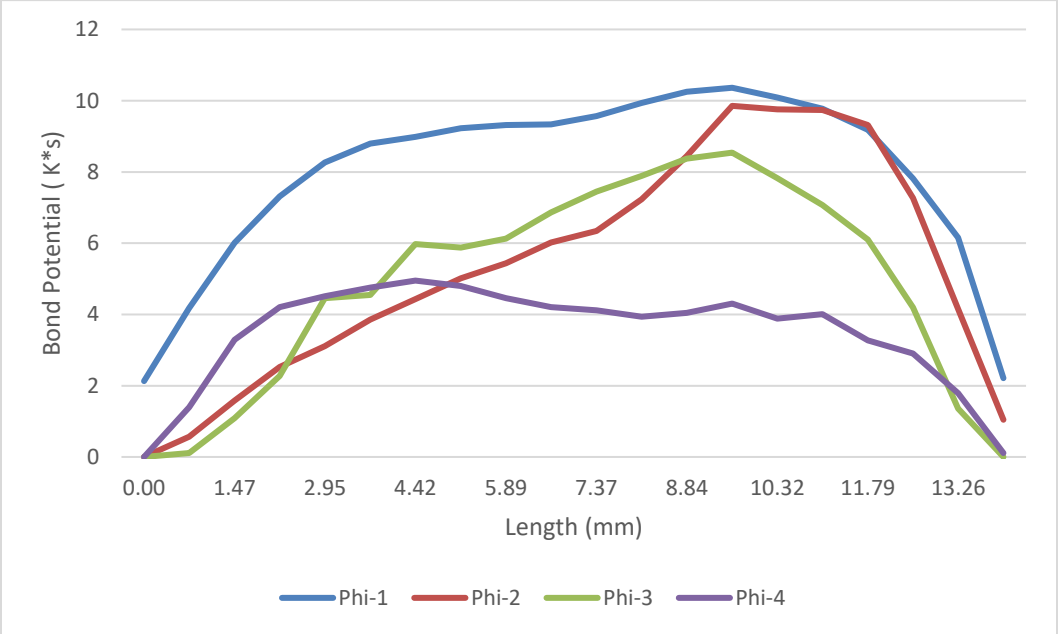

Figure 35: Bond potential for 14 mm bead

Following are the observations from the above results:

1. The comparison between the two bond potential values are significant . There seems to be a lower relationship between the two specimens compared to the two bead and two-layer analysis. However, the common trend that suggests that there is a lower value of the bond potential at the end of the bead and a higher value of the bond potential at the mid-section.
2. It can be observed that the highest value of bond potential for a 7 mm bead is the second layer and for the 14 mm bead, it is the first layer.
3. A sudden spike in the first layer bond potential (Phi-1(7)) marked by point ‘a’ in Figure 34 can be observed. There is no particular explanation of the same at this moment and further investigation needs to be done.
4. The bond potential for the 14 mm bead is very less. One of the major reasons for the same is the lack of temperature history. This is because the time taken for the temperatures to go below critical temperature in 7 mm bead was 6.7 seconds while that for 14 mm bead was 2.3 seconds. Hence, the value of bond potential for 7 mm is way higher than that of 14 mm. Another reason for the same could be that since convective correlation was used, there is a possibility that as the dimensions changed the heat transfer coefficient also changed. Thus, there needs to be further analysis to understand this feature better and to find out its application for this particular scenario.

The following data validates that as the length of the specimen increases, it is exposed to more cooling, which causes faster solidification. The bond potential for 14 mm specimen and 7 mm specimen just like Figure 22 and 23 have lower values at the endpoint. This could imply a stress concentration present at the endpoints, which

suggests that the failure should occur at the endpoints initially and cause crack propagation towards the center of the specimen. In order to do so, an investigation of tensile tests for the two dog bone specimens of 14 mm and 7 mm was performed. Each specimen has equal thickness resembling the revised model explained in section 4.5

4.6 Tensile tests for dog bone specimens:

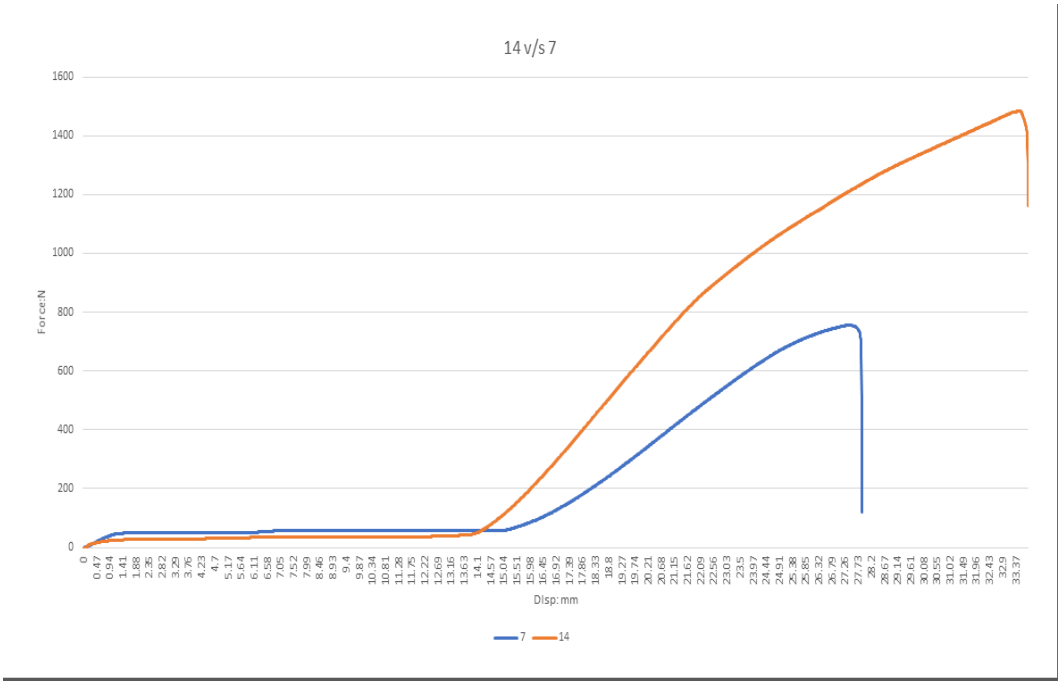

Figure 36: Tensile test for 14 mm and 7 mm specimen

Tensile tests for both the specimens were carried out for 14 mm and 7 mm specimen. The results clearly show that the 14 mm specimen fails at a higher force than 7 mm, implying that the 14 mm specimen has higher strength. In order to find out a relation between the bond potential and the tensile test, we compared the minimum, maximum and average values.

Table 7: Comparison between values of tensile test and bond potential

Sr No.	Tensile test	Force (N)		Bond Potential (K*s)		
		7 mm	14 mm		7 mm	14 mm
1	Average	233.514	537.9705	Average	57.18546	5.38644
2	Maximum	755.285	1484.171	Maximum	77.84881	10.36327
3	Minimum	0.050068	0.046889	Minimum	16.21546	0

From the table, it is clear that there is no particular quantitative relationship between tensile tests and bond potential calculation yet. Hence there needs to be further investigation to obtain the same.

In order to validate the theory of crack propagation from endpoints to mid-section, the failure point needs to be captured using a slow-motion camera with high precision. The specimens also need to be observed carefully under the microscope to investigate the failures intrinsically. Finally, the stress values between the two specimens also need to be calculated to obtain a quantitative relationship with the bond potential, so as to bridge thermal parameters with mechanical strength.

Chapter 5 Conclusion

In the following thesis, an effort was taken to find out a relationship between thermal and mechanical properties of an FDM part. The medium through which the investigation performed involved calculation of the bond potential and understand its behavior between two specimens of varying lengths. During the process, the importance of finding the interface temperature at any instance was a key challenge. An attempt to calculate the same was done using FEM. It was observed that the heat transfer coefficient is an important parameter while investigating the interface temperature. The proposed model does not account for certain factors like the nozzle effect and hysteresis but is fairly acceptable. Further investigation needs to be done to accurately account for all the factors in the model to match the experimental and FEM data.

It was observed that the calculation of bond potential has the ability to predict stress concentrations at the exterior points of any FDM part. The heat transfer coefficient is a major influencer which can control the value of bond potential. Furthermore, comparison of the bond potential between two specimens needs to be done under heat transfer coefficients. Thus, it becomes imperative to investigate the appropriate heat transfer coefficient during the analysis.

The tensile specimens do not show a quantitative relationship with the bond potential yet. There needs to be further investigation to optimize the calculation of bond potential and compare extensively to provide a quantitative relationship.

Chapter 6 Future work:

Future work towards this research would be to incorporate the accurate physics of the FDM seamlessly and to aim a quantitative relationship between the bond potential and strength.

1. Automate the current FEM model and avoid manual updates in the boundary conditions. The analyses carried out were done manually. Even though a single analysis took on an average of about 2 minutes, with the change in complexity, the time increases causing large overall time.
2. Research must be done to understand the behavior of viscoelastic polymers; especially the behavior of the heat transfer coefficient. This could be done by understanding the convection phenomenon in detail.
3. To incorporate CFD and thermal transient analysis as a multiphysics to obtain accurate results for the temperature measurement. This would require high computational power. At this moment, COMSOL Multiphysics can be used as an effective platform to achieve this.
4. The bond potential in this thesis was carried out for the center of the width of the specimens. The results imply the presence of lower bond potential at the exterior due to convection. Hence it is imperative to analyze the bond potential at the exterior ends along the width of the specimen.
5. The tensile specimen needs to be observed under the microscope and the failure needs to be captured in slow-motion to understand failure process intrinsically. This would validate the phenomenon about bond potential and the reason for its lower values at the exterior end.

References

[1] ASTM International, F2792-12a - Standard Terminology for Additive Manufacturing Technologies. 2013.

[2] Gibson, I., Rosen, D.W. and Stucker, B. (2013), Additive Manufacturing Technologies: Rapid Prototyping to Direct Digital Manufacturing, Springer, New York, NY.

[3] ASTM, 2009, ASTM International Committee F42 on Additive Manufacturing Technologies, ASTM F2792–10 Standard Terminology for Additive Manufacturing Technologies, ASTM, West Conshohocken, PA.

[4] B. N. Turner, R. Strong, and S. A. Gold, “A review of melt extrusion additive manufacturing processes: I. Process design and modeling,” Rapid Prototype. J., vol. 20, no. 3, pp. 192–204, 2014.

[5] 3Dprinting failures [Online]. Available: http://www.3dprinterworld.com/sites/speh/files/images/3dp-fails/fredinicalibration1.jpg. [Accessed 6th August 2018]

[6] Wohlers, T.T. (2011), Wohlers Report 2011: Additive Manufacturing and 3D Printing State of the Industry Annual Worldwide Progress Report, Wohlers Associates, Inc., Fort Collins, CO.

[7] Popularity of FDM [Online] https://wohlersassociates.com/blog/2016/01/popularity-of-fdm/.[Accessed 4th August 2018]

[8] Case study Volvo [online] Available: http://www.stratasys.com/resources/search/case-studies/volvo. [Accesed 07/23/2018]

[9] Optimized Production for Agile Manufacturing [online] Available: http://www.stratasys.com/resources/search/ebooks/fortus-advantage. [Accessed: 8th August 2018

[10] Y. Huang, M. C. Leu, J. Mazumder, and A. Donmez, 2015,“Additive Manufacturing: Current State, Future Potential, Gaps and Needs, and Recommendations,” J. Manuf. Sci. Eng., vol. 137, no. 1, p. 014001,

[11] Ultem 9095 [Online]. Available: PLA [Online]. Available: (http://www.stratasys.com/materials/search/pla). [Accessed 6th August 2018] . [Accessed 6th August 2018]

[12] M. K. Agarwala, V. R. Jamalabad, N. A. Langrana, A. Safari, P. J. Whalen, and S. C. Danforth, “Emerald Article : Structural quality of parts processed by fused deposition Structural quality of parts processed by fused deposition,” vol. 2, pp. 1–15, 1996.

[13] ABS m30i [Online]. Available:(http://www.stratasys.com/materials/search/abs-m30i)[Accessed 6th August,2018)

[14] ABSi[Online]. Available:(http://www.stratasys.com/materials/search/absi [Accessed 6th August,2018)

[15] ABS-m30[Online]. Available: ABS m30(http://www.stratasys.com/materials/search/abs-m30) [Accesed 6th August 2018)

[16] PLA [Online]. Available: (http://www.stratasys.com/materials/search/pla). [Accessed 6th August 2018]

[17] Rosenzweig, N. and Narkis, M. (1981), “Sintering rheology of amorphous polymers”, Polymer Engineering and Science, Vol. 21, pp. 1167-1170

[18] ABS [Online]. Available:https://reprap.org/wiki/ABS. Accessed 7th August 2018

[19] M. a Yardimci and S. Güçeri, “Conceptual framework for the thermal process

modeling of fused deposition," Rapid Prototype. J., vol. 2, no. 2, pp. 26–31, 1996.
[20] J. P. Thomas and J. F. Rodriguez, "Modeling the Fracture Strength Between Fused-Deposition Extruded Roads," Solid Free. Fabr. Proc., pp. 17–23, 2000.
[21] P. Central, "Modeling of Bond Formation Between Polymer Filaments in the Fused Deposition Modeling Process," 2004.
[22] Q. Sun, G. M. Rizvi, C. T. Bellehumeur, and P. Gu, "Effect of processing conditions on the bonding quality of FDM polymer filaments," Rapid Prototype. J., vol. 14, no. 2, pp. 72–80, 2008.
[23] Mechanical Characterization of 3D-Printed Polymers - Scientific Figure on ResearchGate. Available from: https://www.researchgate.net/FDM-setup-243_fig5_321702417 [Accessed 4th Aug 2018]
[24] Dillon, H. E. *et al.* (2010) 'Dimensionless versus Dimensional Analysis in CFD and Heat Transfer'.
[25] P. Operation, P. Cleaning, M. Components, F. Switches, and C. Requirements, "User Manual," 2018.
[26] Modeling Convective heat [Online]. Available: https://www.comsol.com/blogs/modeling-natural-and-forced-convection-in-comsol-multiphysics/. [Accessed 25th July 2018]
[27] D. Ravoori, H. Prajapati, C. Lowery, A. Jain, 'Experimental and Theoretical Investigation of Heat Transfer in Platform Bed during Polymer Extrusion-Based Additive Manufacturing, 'Additive Manufacturing, in a review, 2018.
[28] Costa, S. F., Duarte, F. M. and Covas, J. A. (2017) 'Estimation of filament temperature and adhesion development in fused deposition techniques', Journal of Materials Processing Technology, 245, pp. 167–179. doi: 10.1016/j.jmatprotec.2017.02.026.
[29] COMSOL Multiphysics Reference Manual, version 5.2a", COMSOL, Inc, www.comsol.com

Biographical Information

Junaid Mohamed Farooque Baig completed his Bachelor of Engineering (B.E) degree in Mechanical Engineering from Mumbai University, Mumbai, Maharashtra, India. He joined the Department of Mechanical and Aerospace Engineering at University of Texas at Arlington in August 2016 as a graduate student and earned his Master of Science degree in Mechanical Engineering in August 2018.